

Analytic NNLO QCD corrections to top quark pair production in electron-positron collisions

Long-Bin Chen², Jian Wang^{3,4}, Yefan Wang¹

¹*Department of Physics and Institute of Theoretical Physics, Nanjing Normal University, Nanjing, Jiangsu 210023, China*

²*School of Physics and Materials Science, Guangzhou University, Guangzhou 510006, China*

³*School of Physics, Shandong University, Jinan, Shandong 250100, China*

⁴*Center for High Energy Physics, Peking University, Beijing 100871, China*

ABSTRACT: We present the analytic total cross section of top quark pair production in electron-positron annihilation at next-to-next-to-leading order (NNLO) in Quantum Chromodynamics (QCD). By utilizing the optical theorem, the NNLO corrections are related to the imaginary parts of three-loop self-energy Feynman diagrams, of which the master integrals are calculated with canonical differential equations. The analytic results for the NNLO corrections are expressed in terms of multiple polylogarithms as well as elliptic functions. We discuss the asymptotic expansions near the threshold and in the high energy limit in detail. Numerical results are provided for the total cross section of top quark pair production at future lepton colliders.

Contents

| | | |
|----------|---|-----------|
| 1 | Introduction | 1 |
| 2 | Calculation framework | 2 |
| 3 | Calculation of master integrals | 6 |
| 3.1 | Canonical basis of the P2 family | 7 |
| 3.2 | Canonical basis of the P3 family | 8 |
| 3.3 | Boundary conditions | 10 |
| 4 | Analytical NNLO QCD corrections | 10 |
| 5 | Asymptotic expansion | 16 |
| 6 | Numerical results | 19 |
| 7 | Conclusion | 23 |
| A | Topologies of the master integrals | 23 |

1 Introduction

As the heaviest particle in the standard model (SM) of particle physics, the top quark plays a special role in the precise test of the SM and the exploration of energy frontiers [1]. Since its discovery [2, 3], the top quark has attracted continuous research interest. The top quarks can be copiously produced in pairs via strong interactions at the large hadron collider. This process provides the dominant background in searching for the signal of new physics, and can also be used to determine the strong coupling and parton distribution functions. The top quark mass has been measured to be 172.52 ± 0.33 GeV by utilizing the top quark pair events [4]. The single top quark production is also an important process at the large hadron collider which can be used to extract the CKM matrix element V_{tb} and to set constraints on the anomalous Wtb couplings [5].

The future lepton colliders provide more accurate probes to the top quark properties. The cross section of top quark pair production near the threshold is so sensitive to the top quark mass and width that they can be determined with unprecedented precision [6, 7]. The top quark pair production above the threshold can also be used to measure the top quark mass [6]. Moreover, the $tt\gamma$ and ttZ couplings, which get only loss constraints at hadron colliders, can be measured precisely via this process [8, 9], since the top quark pair production is induced by electroweak interaction at lepton colliders.

To match the experimental precision, higher-order QCD and electroweak corrections have to be included. The cross section near the top quark pair threshold has been calculated up to QCD next-to-next-to-next-to-leading order (NNNLO) [10–14]. The theoretical uncertainty is reduced to $\pm 3\%$. The cross section above the threshold receives a number of quantum corrections. The NLO QCD and electroweak corrections were obtained in refs. [15, 16] and refs.[17, 18], respectively. The NNLO QCD corrections were first computed with the small mass expansion method [19–21], and then achieved with full mass dependence by numerical integration methods to properly subtract the infrared divergences [22–25]. The flavor non-singlet NNNLO contribution was investigated using the Padé approximation method [26, 27]. Recently, the full NNNLO QCD corrections were calculated in the form of piecewise functions which are written as a power series [28]. Discussion on the improvement of renormalization scale dependence using the principle of maximum conformality was carried out in [29].

In this paper, we are going to present the full QCD NNLO analytic result of top quark pair production at a future lepton collider. This is made possible thanks to the recent improvement in the analytic method of calculating Feynman integrals, especially the proper choice of a canonical basis for the differential equations satisfied by the Feynman integrals [30]. Our analytic result enables an efficient computation of the total cross section of top quark pair production at any collider energy. The various limits, such as in the threshold or high energy regions, can be investigated with deep expansion of the full result, which may provide valuable insights into the construction of the corresponding effective theories. Besides, we provide analytic results for the master integrals with massive propagators, which are useful for understanding the symbol and (pseudo-)pole structure of general loop integrals.

The rest of this paper is organized as follows. In section 2, we set up the relation between the total cross section of $e^-e^+ \rightarrow t\bar{t}$ and the forward scattering amplitude of a vector boson, and introduce the coupling structure of top quark pair production and the workflow of our calculation. The master integrals needed in this process are computed using the method of differential equations in section 3. Then we present analytical results for various contributions to the NNLO QCD corrections in section 4. The asymptotic expansions in the threshold and high energy limits are discussed in detail in section 5, and the numerical results are exhibited in section 6. We conclude in section 7.

2 Calculation framework

We make use of the optical theorem to calculate QCD higher-order corrections to the total cross section of $e^-e^+ \rightarrow \gamma^*/Z^* \rightarrow t\bar{t}$,

$$\sigma_{e^-e^+ \rightarrow t\bar{t}} = \frac{1}{4s} \text{Im}[e^-(p_1)e^+(p_2) \rightarrow V^\mu(k) \rightarrow t\bar{t} \rightarrow V'^\nu(k) \rightarrow e^-(p_1)e^+(p_2)], \quad (2.1)$$

where $s = k^2 = 2p_1 \cdot p_2$ and the factor $1/4$ is due to the polarization average of the initial states, V and V' could be γ or Z bosons. We have taken top quarks as the heavy quarks, but it is ready to extend the results to the other heavy quarks. The initial- and final-state

electron (positron) have the same momenta and spins, and therefore one can take traces over the lepton fermion chain, obtaining

$$L_{VV'}^{\mu\nu} = c_0^{VV'} (-sg^{\mu\nu} + 2p_1^\mu p_2^\nu + 2p_1^\nu p_2^\mu), \quad (2.2)$$

where

$$c_0^{\gamma\gamma} = 8\pi\alpha, \quad c_0^{ZZ} = \frac{8\pi\alpha (c_{\text{axi}}^2 + c_{\text{vec,l}}^2)}{\sin^2 \theta_W}, \quad c_0^{\gamma Z} = \frac{8\pi\alpha c_{\text{vec,l}}}{\sin \theta_W} \quad (2.3)$$

with the couplings between the Z boson and leptons

$$c_{\text{axi}} = -\frac{1}{4\cos\theta_W}, \quad c_{\text{vec,l}} = c_{\text{axi}} (1 - 4\sin^2\theta_W). \quad (2.4)$$

The QCD corrections exist only in the quark sector $V^\mu(k) \rightarrow t\bar{t} \rightarrow V'^\nu(k)$, of which the amplitude takes the form

$$H_{\mu\nu}^{VV'} = c_1^{VV'} g_{\mu\nu} + c_2^{VV'} k_\mu k_\nu. \quad (2.5)$$

The second term does not contribute due to the identity $k_\mu L_{VV'}^{\mu\nu} = 0$. Then the cross section is given by

$$\sigma_{e^-e^+\rightarrow t\bar{t}} = \sum_{V,V'=\gamma,Z} -\frac{1}{2} c_0^{VV'} \text{Im}_{t\bar{t}}[c_1^{VV'}] \times \frac{1}{s - m_V^2 + im_V \Gamma_V} \frac{1}{s - m_{V'}^2 - im_{V'} \Gamma_{V'}}, \quad (2.6)$$

where $\Gamma_{V,V'}$ is the decay width of the vector boson and $\text{Im}_{t\bar{t}}[c_1^{VV'}]$ denotes the imaginary part of $c_1^{VV'}$ induced by the cuts on at least a top quark pair.

In the following part, we focus on the calculation of $c_1^{VV'}$, which can be obtained from $H_{\mu\nu}^{VV'}$ by

$$c_1^{VV'} = \frac{1}{d-1} \left(g^{\mu\nu} H_{\mu\nu}^{VV'} - \frac{1}{s} k^\mu k^\nu H_{\mu\nu}^{VV'} \right). \quad (2.7)$$

Because the intermediate vector bosons V, V' can be either a photon or a Z boson, the cross section is decomposed to three parts,

$$\sigma_{e^-e^+\rightarrow t\bar{t}} = \sigma_{e^-e^+\rightarrow t\bar{t}}^{\gamma\gamma} + \sigma_{e^-e^+\rightarrow t\bar{t}}^{ZZ} + \sigma_{e^-e^+\rightarrow t\bar{t}}^{\gamma Z}, \quad (2.8)$$

where the superscripts denote the intermediate vector bosons. We consider QCD higher-order corrections, and expand the cross section in a series of the strong coupling α_s ,

$$\sigma_{e^-e^+\rightarrow t\bar{t}}^{VV'} = \sigma_{\text{LO}}^{VV'} \left(1 + \frac{\alpha_s}{\pi} X_1^{VV'} + \left(\frac{\alpha_s}{\pi} \right)^2 X_2^{VV'} + \mathcal{O}(\alpha_s^3) \right). \quad (2.9)$$

The leading order (LO) results read

$$\sigma_{\text{LO}}^{\gamma\gamma} = \frac{4\pi\alpha^2 C_A e_u^2 \sqrt{s(s-4m_t^2)} (s+2m_t^2)}{3s^3}, \quad (2.10)$$

$$\sigma_{\text{LO}}^{ZZ} = \frac{4\pi\alpha^2 C_A \left(c_{\text{axi}}^2 + c_{\text{vec},l}^2 \right) \sqrt{s(s-4m_t^2)} \left(c_{\text{axi}}^2 (s-4m_t^2) + c_{\text{vec},u}^2 (s+2m_t^2) \right)}{3 \sin^4 \theta_W s \left((s-m_Z^2)^2 + m_Z^2 \Gamma_Z^2 \right)}, \quad (2.11)$$

$$\sigma_{\text{LO}}^{\gamma Z} = -\frac{8\pi\alpha^2 C_A c_{\text{vec},u} c_{\text{vec},l} e_u \sqrt{s(s-4m_t^2)} (s+2m_t^2) (s-m_Z^2)}{3 \sin^2 \theta_W s^2 \left((s-m_Z^2)^2 + m_Z^2 \Gamma_Z^2 \right)}, \quad (2.12)$$

where e_u and m_t are the charge and mass of the top-quark, m_Z and Γ_Z represent the mass and width of the Z boson, θ_W is the weak mixing angle, and the couplings between the Z boson and quarks are given by

$$c_{\text{vec},u} = -c_{\text{axi}} \left(1 - \frac{8}{3} \sin^2 \theta_W \right), \quad c_{\text{vec},d} = c_{\text{axi}} \left(1 - \frac{4}{3} \sin^2 \theta_W \right). \quad (2.13)$$

The NLO QCD corrections were computed in refs. [15, 17]. We have calculated them independently and obtained

$$\begin{aligned} X_1^{ZZ} &= \frac{c_{\text{vec},u}^2 C_F}{4(w-1)^3(w+1) \left(c_{\text{axi}}^2 (w+1)^2 + c_{\text{vec},u}^2 (w^2-4w+1) \right)} \times \\ &\left[8(w-1)^2 (w^2+1) (w^2-4w+1) \right. \\ &\times (-2G(-1,0,w) + 2G(0,-1,w) + G(0,1,w) - G(1,0,w)) \\ &+ 8(w-1)^2 (w^2-4w+1) (i\pi w^2 - w^2 + i\pi + 1) (2G(-1,w) + G(1,w)) \\ &+ 4(w-1)^2 w (6w^3 - 22w^2 + 7w + 2) G(0,w) \\ &\left. + (w-1)^2 (3(1-8i\pi)w^4 + (-24+88i\pi)w^3 - 28i\pi w^2 + 8(3-i\pi)w - 3) \right] \\ &+ \frac{c_{\text{axi}}^2 C_F}{4(w-1)^3(w+1) \left(c_{\text{axi}}^2 (w+1)^2 + c_{\text{vec},u}^2 (w^2-4w+1) \right)} \times \\ &\left[8(-w^6 + w^4 + w^2 - 1) G(1,0,w) - 8(w-1)^2 (w+1)^2 (w^2+1) \right. \\ &\times (2G(-1,0,w) - 2G(0,-1,w) - G(0,1,w)) \\ &+ 8(w-1)^2 (w+1)^2 (i\pi w^2 - w^2 + i\pi + 1) (2G(-1,w) + G(1,w)) \\ &+ 4w (6w^5 - 7w^4 - 3w^3 - 10w^2 + 15w - 7) G(0,w) \\ &+ 3(1-8i\pi)w^6 + 4(6+7i\pi)w^5 + (-45+12i\pi)w^4 + 40i\pi w^3 \\ &\left. + 15(3-4i\pi)w^2 + 4i(7\pi+6i)w - 3 \right], \quad (2.14) \end{aligned}$$

where the redefinition of the parameter

$$z = -\frac{(w-1)^2}{w} \quad (2.15)$$

has been used to rationalized the square root $\sqrt{z(z-4)}$ with $-1 \leq w < 0$ assuming $z \geq 4$. The multiple polylogarithms (MPLs) [31] are defined by $G(x) \equiv 1$ and

$$G(l_1, l_2, \dots, l_n, x) \equiv \int_0^x \frac{dt}{t-l_1} G(l_2, \dots, l_n, t), \quad (2.16)$$

$$G(\vec{0}_n, x) \equiv \frac{1}{n!} \ln^n x. \quad (2.17)$$

The number of elements in the set $\{l_1, l_2, \dots, l_n\}$ is referred to as the transcendental *weight* of the MPLs.

One can see that there are both vector and axial-vector contributions in X_1^{ZZ} . But $X_1^{\gamma\gamma}$ and $X_1^{\gamma Z}$ only have vector contributions,

$$X_1^{\gamma\gamma} = X_1^{\gamma Z} = X_1^{ZZ} \Big|_{c_{\text{axi}}=0}. \quad (2.18)$$

To calculate the NNLO QCD corrections, we need to consider the three-loop Feynman diagrams of $V \rightarrow t\bar{t} \rightarrow V'$. Some typical diagrams are shown in figure 1 and figure 2. Figure 1(a) shows the flavor non-singlet contribution, which is induced either by a vector or axial-vector current. Figure 1(b) and (c) represent the flavor singlet contribution, in which only axial-vector currents give non-vanishing results. In the diagrams in figure 1, the top quark couples to the electroweak boson, and thus these contributions are denoted by $X_{2,Vt\bar{t}}$. In the diagrams in figure 2, the top quark does not enter the electroweak current directly but arises from a gluon splitting, and the corresponding contributions are labelled by $X_{2,g\bar{t}\bar{t}}$. Notice that diagrams in figure 1(b) and (c) and figure 2 start from NNLO QCD corrections.

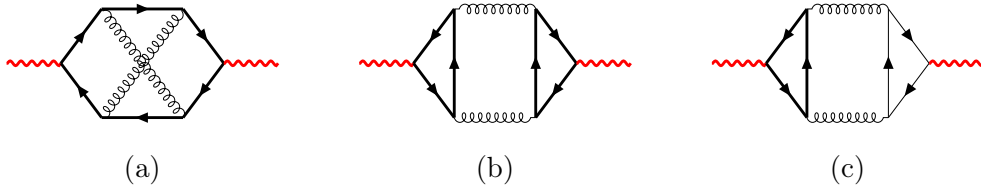


Figure 1: Typical three-loop Feynman diagrams of $V \rightarrow t\bar{t} \rightarrow V'$ contributing to $X_{2,Vt\bar{t}}$. The thick black and red wavy lines stand for the massive top quark and the vector boson, respectively. The thin lines represent the massless fermions. The curly lines denote gluons.



Figure 2: Typical three-loop Feynman diagrams of $V \rightarrow t\bar{t} \rightarrow V'$ contributing to $X_{2,g\bar{t}\bar{t}}$. The thick black and red wavy lines stand for the massive top quark and the vector boson, respectively. The thin lines represent the massless fermions. The curly lines denote gluons.

We have generated all the Feynman diagrams and amplitudes of $V^\mu \rightarrow t\bar{t} \rightarrow V^{\nu}$ by FeynArts [32], and simplified the Dirac matrices with FeynCalc [33, 34]. We work in $(4 - 2\epsilon)$ -dimensional space-time to regularize the infrared and ultraviolet divergences. The treatment of γ_5 in dimensional regularization is subtle. For the flavour non-singlet diagrams, such as the one in figure 1(a), we simply use the naive anticommutative γ_5 scheme. The

fermion chain with two γ_5 matrices is easy to deal with since they can be moved together and contracted by $\gamma_5^2 = 1$. The fermion chain with a single γ_5 matrix needs a specific prescription to evaluate the trace generally. In our case, the trace must be proportional to $\epsilon^{\mu\nu\rho\sigma} \times (d_1 k_\rho k_\sigma + d_2 g_{\rho\sigma})$ after loop momentum integrations and thus vanishes, irrespective of the values of the coefficients d_1, d_2 . For the flavour singlet diagrams, such as the one in figure 1(b), we adopt the Larin scheme to deal with the γ_5 matrix [35, 36] and substitute

$$\gamma^\mu \gamma_5 = \frac{i}{3!} \epsilon^{\mu\nu\rho\sigma} \gamma_\nu \gamma_\rho \gamma_\sigma \quad (2.19)$$

in a fermion chain. The Dirac matrices on the right-hand side of the above equation should be taken in $(4 - 2\epsilon)$ dimensions. Notice that since the axial-vector current anomalies in figure 1(b) and (c) appear for the first time at $\mathcal{O}(\alpha_s^2)$, one does not need to consider the (either ultraviolet or finite) renormalization constants of the axial-vector current.

From the amplitudes, we projected out the scalar coefficient c_1 making use of eq. (2.7). Then, all the integrals in c_1 were reduced to a set of master integrals using FIRE [37] and Kira [38]. These master integrals belong to four integral families, which are shown in figure 3. The analytical results of master integrals in the P1 and NP1 families have been derived in our previous work on $H \rightarrow b\bar{b}$ [39]. In the next section, we present the results for the other two integral families.

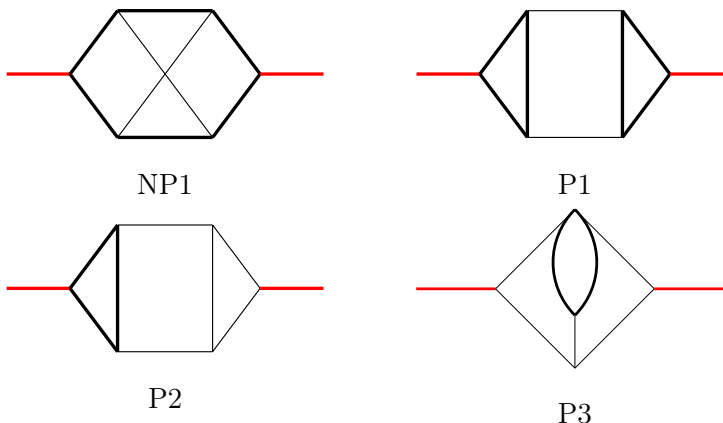


Figure 3: The topologies of master integral families. The thick black and red lines stand for the massive top quark and the vector boson, respectively. The other lines represent massless particles. A cut on at least a top quark pair is assumed.

3 Calculation of master integrals

We calculate the master integrals with the method of differential equations [40, 41]. After choosing a proper basis, the differential equation exhibits a canonical form [30], i.e., the dimensional parameter ϵ is factorized out. Then the solution as a series of ϵ can be found using iterated integrals. In some cases, the kinematic dependence in the differential equation can be represented by logarithmic functions, and the result is expressed in terms of multiple

polylogarithms (MPLs) [31]. We have obtained the canonical differential equations for the P1 and NP1 families in ref. [39]. Below we show the results for the P2 and P3 families.

3.1 Canonical basis of the P2 family

The integrals of the P2 family in figure 3 are defined by

$$I_{n_1, n_2, \dots, n_9}^{\text{P2}} = \text{Im}_{t\bar{t}} \int \mathcal{D}^D q_1 \mathcal{D}^D q_2 \frac{D_9^{-n_9}}{D_1^{n_1} D_2^{n_2} D_3^{n_3} D_4^{n_4} D_5^{n_5} D_6^{n_6} D_7^{n_7} D_8^{n_8}} \quad (3.1)$$

with

$$\mathcal{D}^D q_i = \frac{(m_t^2)^\epsilon}{i\pi^{D/2}\Gamma(1+\epsilon)} d^D q_i, \quad D = 4 - 2\epsilon, \quad (3.2)$$

where all $n_i \geq 0, i = 1, \dots, 8$, and $n_9 \leq 0$. The denominators D_i read

$$\begin{aligned} D_1 &= q_3^2, & D_2 &= (q_3 - k)^2, & D_3 &= q_1^2 - m_t^2, \\ D_4 &= (q_1 + k)^2 - m_t^2, & D_5 &= (q_1 - q_2)^2 - m_t^2, & D_6 &= q_2^2, \\ D_7 &= (q_2 + q_3)^2, & D_8 &= (q_2 + k)^2, & D_9 &= (q_1 + q_3)^2, \end{aligned} \quad (3.3)$$

where the Feynman prescription $+i\epsilon$ has been suppressed. The external momentum k satisfies $k^2 = s$. In the above definition of integrals, we have required only the imaginary contribution induced by a cut on at least a top quark pair.

In the P2 integral family, there are sixteen master integrals contributing to $X_{2,Vt\bar{t}}$. To construct the canonical basis, we first select

$$\begin{aligned} M_1^{\text{P2}} &= \epsilon^3 m_t^2 I_{0,2,2,0,2,0,1,0,0}^{\text{P2}}, & M_2^{\text{P2}} &= \epsilon^3 m_t^2 I_{0,2,2,0,1,0,2,0,0}^{\text{P2}}, \\ M_3^{\text{P2}} &= (1 - 2\epsilon) \epsilon m_t^4 I_{0,1,3,0,3,0,1,0,0}^{\text{P2}}, & M_4^{\text{P2}} &= \epsilon^3 m_t^4 I_{2,1,2,1,2,0,0,0,0}^{\text{P2}}, \\ M_5^{\text{P2}} &= \epsilon^3 m_t^4 I_{2,1,0,2,2,1,0,0,0}^{\text{P2}}, & M_6^{\text{P2}} &= \epsilon^3 m_t^4 I_{2,1,0,2,1,2,0,0,0}^{\text{P2}}, \\ M_7^{\text{P2}} &= (1 - 2\epsilon) \epsilon^3 m_t^2 I_{2,0,1,1,2,0,1,0,0}^{\text{P2}}, & M_8^{\text{P2}} &= \epsilon^3 m_t^4 I_{0,2,2,1,0,2,1,0,0}^{\text{P2}}, \\ M_9^{\text{P2}} &= (1 - 2\epsilon) \epsilon^3 m_t^2 I_{0,1,0,2,1,2,1,0,0}^{\text{P2}}, & M_{10}^{\text{P2}} &= (1 - 2\epsilon) \epsilon^4 m_t^2 I_{1,1,0,2,1,1,1,0,0}^{\text{P2}}, \\ M_{11}^{\text{P2}} &= (1 - 2\epsilon) \epsilon^4 m_t^2 I_{1,1,1,1,2,0,1,0,0}^{\text{P2}}, & M_{12}^{\text{P2}} &= (1 - 2\epsilon) \epsilon^3 m_t^4 I_{1,1,2,1,2,0,1,0,0}^{\text{P2}}, \\ M_{13}^{\text{P2}} &= (1 - 2\epsilon) \epsilon^3 m_t^4 I_{1,1,1,1,3,0,1,0,0}^{\text{P2}}, & M_{14}^{\text{P2}} &= (1 - 2\epsilon) \epsilon^4 m_t^2 I_{0,2,1,1,1,1,1,0,0}^{\text{P2}}, \\ M_{15}^{\text{P2}} &= \epsilon^3 m_t^6 I_{1,2,2,1,0,2,0,1,0}^{\text{P2}}, & M_{16}^{\text{P2}} &= (1 - 2\epsilon) \epsilon^4 m_t^4 I_{2,1,1,1,1,1,0,1,0}^{\text{P2}}. \end{aligned} \quad (3.4)$$

Here all M_i^{P2} are dimensionless, and the corresponding topology diagrams are displayed in figure 7 in appendix A.

Then the canonical basis integrals $F_i^{\text{P2}}, i = 1, \dots, 16$, can be constructed as linear combinations of M_i^{P2} using a method similar to that in ref. [42]. Examples can be found in [43]. For simplicity, we define a dimensionless variable $z \equiv s/m_t^2 + i0^+$. Then we obtain the following canonical basis of the P2 family:

$$\begin{aligned} F_1^{\text{P2}} &= M_1^{\text{P2}}(-z), & F_2^{\text{P2}} &= -(M_1^{\text{P2}} + M_2^{\text{P2}}) r_1, & F_3^{\text{P2}} &= -\frac{1}{4} M_2^{\text{P2}}(4 - z) + M_3^{\text{P2}}, \\ F_4^{\text{P2}} &= M_4^{\text{P2}} r_1(-z), & F_5^{\text{P2}} &= M_5^{\text{P2}} z^2, & F_6^{\text{P2}} &= \frac{1}{2} M_5^{\text{P2}} r_1 z + M_6^{\text{P2}} r_1 z, \end{aligned}$$

$$\begin{aligned}
F_7^{\text{P2}} &= -\frac{M_1^{\text{P2}} r_1 (7z - 12)}{12(4 - z)} + \frac{M_2^{\text{P2}} r_1}{12} - \frac{M_3^{\text{P2}} r_1}{3(4 - z)} + \frac{M_7^{\text{P2}} r_1}{4 - z}, & F_8^{\text{P2}} &= M_8^{\text{P2}} r_1 (-z), \\
F_9^{\text{P2}} &= \frac{M_1^{\text{P2}} r_1}{3} + \frac{M_2^{\text{P2}} r_1 (4 - z)}{6z} - \frac{2M_3^{\text{P2}} r_1}{3z} - \frac{M_5^{\text{P2}} r_1 z}{2} + M_9^{\text{P2}} r_1 + M_{10}^{\text{P2}} r_1, \\
F_{10}^{\text{P2}} &= M_{10}^{\text{P2}} z, & F_{11}^{\text{P2}} &= M_{11}^{\text{P2}} (-z), \\
F_{12}^{\text{P2}} &= \frac{M_1^{\text{P2}} r_1}{3} + \frac{M_2^{\text{P2}} r_1 (4 - z)}{6z} - \frac{2M_3^{\text{P2}} r_1}{3z} + \frac{3M_{11}^{\text{P2}} r_1}{2} + M_{12}^{\text{P2}} r_1 + M_{13}^{\text{P2}} r_1, \\
F_{13}^{\text{P2}} &= M_{13}^{\text{P2}} (-z), & F_{14}^{\text{P2}} &= M_{14}^{\text{P2}} (-z), & F_{15}^{\text{P2}} &= M_{15}^{\text{P2}} r_1 z^2, & F_{16}^{\text{P2}} &= M_{16}^{\text{P2}} z^2,
\end{aligned} \tag{3.5}$$

where

$$r_1 = \sqrt{z(z - 4)}. \tag{3.6}$$

To rationalize the square root r_1 , we write

$$z = -\frac{(w - 1)^2}{w} \tag{3.7}$$

with $-1 \leq w < 0$ assuming $z \geq 4$. This choice of w renders the prescription $w + i0^+$ in analytic continuation. Then r_1 is rationalized to

$$r_1 = \frac{(w + 1)(w - 1)}{w}. \tag{3.8}$$

The corresponding differential equations for the canonical basis \mathbf{F}^{P2} become

$$\frac{d\mathbf{F}^{\text{P2}}}{dw} = \epsilon \left(\sum_{i=1}^3 \frac{\mathbf{N}_i^{\text{P2}}}{w - l_i^{\text{P2}}} \right) \mathbf{F}^{\text{P2}} \tag{3.9}$$

with

$$l_1^{\text{P2}} = 0, \quad l_2^{\text{P2}} = 1, \quad l_3^{\text{P2}} = -1, \tag{3.10}$$

and \mathbf{N}_i^{P2} being constant matrices.

3.2 Canonical basis of the P3 family

The master integrals of the P3 integral family in figure 3 are defined by

$$I_{n_1, n_2, \dots, n_9}^{\text{P3}} = \text{Im}_{t\bar{t}} \int \mathcal{D}^D q_1 \mathcal{D}^D q_2 \frac{D_8^{-n_8} D_9^{-n_9}}{D_1^{n_1} D_2^{n_2} D_3^{n_3} D_4^{n_4} D_5^{n_5} D_6^{n_6} D_7^{n_7}} \tag{3.11}$$

with all $n_i \geq 0, i = 1, \dots, 8$, and $n_9 \leq 0$. The denominators D_i read

$$\begin{aligned}
D_1 &= q_1^2, & D_2 &= q_2^2, & D_3 &= (q_1 + q_2)^2, \\
D_4 &= (q_1 + q_2 - q_3)^2 - m_t^2, & D_5 &= q_3^2 - m_t^2, & D_6 &= (q_2 - k)^2, \\
D_7 &= (q_1 + k)^2, & D_8 &= (q_2 - q_3)^2, & D_9 &= (q_3 - k)^2.
\end{aligned} \tag{3.12}$$

As in the case of the P2 family, only the imaginary contributions induced by a cut on at least a top quark pair are required. There are five master integrals in this family. To construct the canonical basis, we first select

$$\begin{aligned}
M_1^{\text{P3}} &= \epsilon^3 m_t^2 I_{0,2,0,2,2,0,1,0,0}^{\text{P3}}, & M_2^{\text{P3}} &= \epsilon^3 m_t^2 I_{0,2,0,2,1,0,2,0,0}^{\text{P3}}, \\
M_3^{\text{P3}} &= (1-2\epsilon)\epsilon m_t^4 I_{0,1,0,3,3,0,1,0,0}^{\text{P3}}, & M_4^{\text{P3}} &= (1-2\epsilon)\epsilon^4 m_t^2 I_{1,1,1,1,1,1,1,0,0}^{\text{P3}}, \\
M_5^{\text{P3}} &= (1-2\epsilon)\epsilon^3 m_t^4 I_{1,1,1,2,1,1,1,0,0}^{\text{P3}}. & &
\end{aligned} \tag{3.13}$$

The corresponding topology diagrams are displayed in figure 8 in appendix A. Then with the help of the `Libra` package [44], we obtain the following canonical basis of the P3 family:

$$\begin{aligned}
F_1^{\text{P3}} &= M_1^{\text{P3}}(-z), & F_2^{\text{P2}} &= -(M_1^{\text{P3}} + M_2^{\text{P3}}) r_1, & F_3^{\text{P3}} &= -\frac{1}{4} M_2^{\text{P2}}(4-z) + M_3^{\text{P3}}, \\
F_4^{\text{P3}} &= M_4^{\text{P3}} z(1-2\epsilon) - 4M_5^{\text{P3}} z \epsilon, \\
F_5^{\text{P3}} &= -\frac{M_1^{\text{P3}} z (6(z+8)\epsilon^2 + 5z\epsilon + z)}{9r_2(2\epsilon+1)} + \frac{M_2^{\text{P3}}(z-4)z(6\epsilon+1)}{18r_2} - \frac{2M_3^{\text{P3}} z (12\epsilon^2 - 8\epsilon - 1)}{9r_2(2\epsilon+1)} \\
&\quad + M_4^{\text{P3}} \left(\frac{r_2 z(4\epsilon-1)}{2(z+4)} - \frac{z^2 \epsilon}{r_2} \right) + \frac{M_5^{\text{P3}} r_2 z(4\epsilon-1)}{3(z+4)}
\end{aligned} \tag{3.14}$$

with

$$r_2 = \sqrt{z(z+4)}. \tag{3.15}$$

Note that the bases F_1^{P3} , F_2^{P3} and F_3^{P3} exist also in the P2 family and that the bases F_4^{P3} and F_5^{P3} are chosen from a reducible sector.

The analytical results of F_4^{P3} and F_5^{P3} depend on two square roots, i.e., r_1 and r_2 . Making use of the `RationalizeRoots` package [45], we have found a change of the differential variable,

$$z = -\frac{(y^2+1)^2}{(y-1)y(y+1)}, \quad 0 < y \leq \sqrt{2}-1, \tag{3.16}$$

so that the above two square roots can be rationalized simultaneously,

$$r_1 = \frac{(y^2+1)(y^2+2y-1)}{(y-1)y(y+1)}, \quad r_2 = \frac{(y^2+1)(y^2-2y-1)}{(y-1)y(y+1)}. \tag{3.17}$$

The corresponding differential equations for the canonical basis \mathbf{F}^{P3} become

$$\frac{d\mathbf{F}^{\text{P3}}}{dy} = \epsilon \left(\sum_{i=1}^9 \frac{N_i^{\text{P3}}}{y - l_i^{\text{P3}}} \right) \mathbf{F}^{\text{P3}} \tag{3.18}$$

with

$$\begin{aligned}
l_1^{\text{P3}} &= 0, & l_2^{\text{P3}} &= 1, & l_3^{\text{P3}} &= -1, & l_4^{\text{P3}} &= i, & l_5^{\text{P3}} &= -i, \\
l_6^{\text{P3}} &= \sqrt{2}+1, & l_7^{\text{P3}} &= -\sqrt{2}+1, & l_8^{\text{P3}} &= \sqrt{2}-1, & l_9^{\text{P3}} &= -\sqrt{2}-1.
\end{aligned} \tag{3.19}$$

In the calculations of $X_{2,g\bar{t}\bar{t}}$, F_4^{P3} and F_5^{P3} are required up to transcendental *weight* four and three, respectively. Then we find that l_i^{P3} , $i = 6, \dots, 9$ do not appear in the expressions of $X_{2,g\bar{t}\bar{t}}$.

3.3 Boundary conditions

Solving the above differential equations, we get analytical results for the basis integrals in terms of MPLs with undetermined constants. These constants can be fixed by using the regularity condition of the integrals on pseudo-poles or by direct analytical calculation at special phase space points. In our case, we find that the constants consist of $\zeta(n)$ and π^n . On the other hand, high-precision numerical results of the constants can be obtained by comparing the analytical results to the numerical results calculated with the `AMFlow` package [46–49]. Then the explicit analytical form is reproduced using the PSLQ algorithm [50]. Specifically, we chose to determine the boundary condition directly in the physical phase space, i.e., $z > 4$, and consider the contributions only from cuts on at least a top quark pair. Therefore, it is unnecessary to consider analytic continuation. We provide analytic results of all the canonical bases in an ancillary file along with this paper.

4 Analytical NNLO QCD corrections

Based on the analytical results of the master integrals, we obtain the results for three-loop contributions to the cross section in eq. (2.6). All the infrared divergences have been canceled. However, there are remaining ultraviolet divergences. They cancel out after including the contributions from counter-terms. The calculation of this part is standard and thus we refrain from giving the details here. The interested readers are referred to ref. [39].

As mentioned in section 2, there are two kinds of diagrams with different coupling structures contributing to the cross section, i.e.,

$$X_2 = X_{2,Vt\bar{t}} + X_{2,g\bar{t}\bar{t}} \quad (4.1)$$

with

$$\begin{aligned} X_{2,Vt\bar{t}} &= X_{2,Vt\bar{t}}^{ZZ} + X_{2,Vt\bar{t}}^{\gamma Z} + X_{2,Vt\bar{t}}^{\gamma\gamma} \\ &\quad + \theta(z - 16) \left[X_{2,Vt\bar{t}}^{ZZ,4t} + X_{2,Vt\bar{t}}^{\gamma Z,4t} + X_{2,Vt\bar{t}}^{\gamma\gamma,4t} \right] \\ X_{2,g\bar{t}\bar{t}} &= X_{2,g\bar{t}\bar{t}}^{ZZ} + X_{2,g\bar{t}\bar{t}}^{\gamma Z} + X_{2,g\bar{t}\bar{t}}^{\gamma\gamma}. \end{aligned} \quad (4.2)$$

In the first equation, we split the contributions according to the number of top (anti-)quarks crossing the cuts. The second line represents the contribution from four top (anti-)quarks, which is non-vanishing only for $z \geq 16$ ($\sqrt{s} \geq 4m_t$). The full analytical results for all the above terms are provided in an ancillary file. Below we present the results of maximal transcendental *weight* explicitly for $X_{2,Vt\bar{t}}$.

$$\begin{aligned} X_{2,Vt\bar{t}}^{ZZ} &= \frac{c_{\text{vec,u}}^2}{(c_{\text{axi}}^2(w+1)^2 + c_{\text{vec,u}}^2(w^2 - 4w + 1))} \\ &\quad \times \left(\frac{4(w^2 + 1)^2(w^2 - 4w + 1)}{9(w^2 - 1)^2} \right) \left[100i\pi G(0, -1, -1, w) + 76i\pi G(0, -1, 1, w) \right. \\ &\quad \left. + 76i\pi G(0, 1, -1, w) + 35i\pi G(0, 1, 1, w) - 100G(0, -1, -1, 0, w) - 28G(0, -1, 0, -1, w) \right] \end{aligned}$$

$$\begin{aligned}
& -14G(0, -1, 0, 1, w) - 76G(0, -1, 1, 0, w) + 128G(0, 0, -1, -1, w) + 64G(0, 0, -1, 1, w) \\
& + 64G(0, 0, 1, -1, w) + 32G(0, 0, 1, 1, w) - 76G(0, 1, -1, 0, w) + 4G(0, 1, 0, -1, w) \\
& + 2G(0, 1, 0, 1, w) - 35G(0, 1, 1, 0, w) \Big] \\
& + \frac{4(8w^4 - 85w^3 + 166w^2 - 85w + 8)}{27(w^2 - 1)} \Big[8\pi^2 G(1, x_1, w) + 12i\pi G(1, x_1, 0, w) \\
& + 3i\pi G(1, x_1, 1, w) + 18G(1, x_1, 0, -1, w) - 12G(1, x_1, 0, 0, w) + 9G(1, x_1, 0, 1, w) \\
& - 3G(1, x_1, 1, 0, w) + 8\pi^2 G(1, x_2, w) + 12i\pi G(1, x_2, 0, w) + 3i\pi G(1, x_2, 1, w) \\
& + 18G(1, x_2, 0, -1, w) - 12G(1, x_2, 0, 0, w) + 9G(1, x_2, 0, 1, w) - 3G(1, x_2, 1, 0, w) \\
& - 3i\pi G(1, 0, 1, w) - 18G(1, 0, 0, -1, w) - 9G(1, 0, 0, 1, w) + 3G(1, 0, 1, 0, w) \Big] \\
& - \frac{2(32w^6 - 181w^5 + 230w^4 - 192w^3 - 86w^2 - 11w + 16)}{27(w^2 - 1)^2} \Big[8\pi^2 G(0, x_1, w) \\
& + 12i\pi G(0, x_1, 0, w) + 3i\pi G(0, x_1, 1, w) + 18G(0, x_1, 0, -1, w) - 12G(0, x_1, 0, 0, w) \\
& + 9G(0, x_1, 0, 1, w) - 3G(0, x_1, 1, 0, w) + 8\pi^2 G(0, x_2, w) + 12i\pi G(0, x_2, 0, w) \\
& + 3i\pi G(0, x_2, 1, w) + 18G(0, x_2, 0, -1, w) - 12G(0, x_2, 0, 0, w) + 9G(0, x_2, 0, 1, w) \\
& - 3G(0, x_2, 1, 0, w) \Big] - \frac{2w(24w^5 - 145w^4 + 182w^3 - 96w^2 - 110w + 49)}{9(w^2 - 1)^2} \\
& \times \Big[2G(0, 0, 0, -1, w) + G(0, 0, 0, 1, w) \Big] \\
& + \frac{4(90w^6 - 671w^5 + 1174w^4 - 872w^3 - 520w^2 - 201w + 128)}{9(w^2 - 1)^2} \\
& \times \Big[G(0, -1, 0, 0, w) - i\pi G(0, -1, 0, w) \Big] \\
& + \frac{w(6w^5 - 23w^4 + 10w^3 - 24w^2 + 8w - 1)}{9(w^2 - 1)^2} \Big[G(0, 0, 0, 0, w) - i\pi G(0, 0, 0, w) \Big] \\
& + \frac{8(24w^6 - 45w^5 - 120w^4 + 32w^3 + 96w^2 + 77w - 32)}{9(w^2 - 1)^2} \\
& \times \Big[G(0, 0, -1, 0, w) - i\pi G(0, 0, -1, w) \Big] \\
& + \frac{4(47w^6 - 111w^5 - 168w^4 + 36w^3 + 141w^2 + 147w - 56)}{9(w^2 - 1)^2} \\
& \times \Big[G(0, 0, 1, 0, w) - i\pi G(0, 0, 1, w) \Big] \\
& + \frac{4(w^4 - 4w^3 + 4w^2 - 4w + 1)}{27(w^2 - 1)} \Big[5\pi^2 G(1, 0, w) + 6i\pi G(1, 0, 0, w) - 6G(1, 0, 0, 0, w) \Big] \\
& + \frac{2(29w^6 - 424w^5 + 1075w^4 - 840w^3 - 445w^2 - 416w + 181)}{9(w^2 - 1)^2} \\
& \times \Big[G(0, 1, 0, 0, w) - i\pi G(0, 1, 0, w) \Big] \\
& - \frac{2\pi^2(361w^6 - 2689w^5 + 4707w^4 - 3488w^3 - 2091w^2 - 799w + 511)}{27(w^2 - 1)^2} G(0, -1, w)
\end{aligned}$$

$$\begin{aligned}
& - \frac{2\pi^2 w (8w^5 - 31w^4 + 16w^3 - 32w^2 + 8w - 1) G(0, 0, w)}{27 (w^2 - 1)^2} \\
& - \frac{2\pi^2 (19w^6 - 281w^5 + 713w^4 - 560w^3 - 293w^2 - 279w + 121) G(0, 1, w)}{9 (w^2 - 1)^2} \\
& - \frac{4i}{9 (w^2 - 1)} \left[\pi^3 (w^4 - 4w^3 + 4w^2 - 4w + 1) \right. \\
& - 3i (8w^4 - 85w^3 + 166w^2 - 85w + 8) \zeta(3) \left. \right] G(1, w) \\
& - \frac{1}{27 (w^2 - 1)^2} \left[6 (15w^6 - 61w^5 + 53w^4 - 64w^3 - 5w^2 - 3w + 1) \zeta(3) \right. \\
& - i\pi^3 w (10w^5 - 39w^4 + 22w^3 - 40w^2 + 8w - 1) \left. \right] G(0, w) \\
& + \frac{\pi^4 (231w^6 - 873w^5 + 285w^4 - 848w^3 + 351w^2 + 25w - 19)}{1620 (w^2 - 1)^2} \\
& + \frac{2i\pi (15w^6 - 61w^5 + 53w^4 - 64w^3 - 5w^2 - 3w + 1) \zeta(3)}{9 (w^2 - 1)^2} \\
& + \frac{c_{\text{axi}}^2}{(c_{\text{axi}}^2 (w + 1)^2 + c_{\text{vec,u}}^2 (w^2 - 4w + 1))} \\
& \times \left(\frac{4 (8w^4 - 35w^3 + 190w^2 - 35w + 8)}{27 (w^2 - 1)} \left[8\pi^2 G(1, x_1, w) + 8\pi^2 G(1, x_2, w) \right. \right. \\
& - 3i\pi G(1, 0, 1, w) + 12i\pi G(1, x_1, 0, w) + 3i\pi G(1, x_1, 1, w) + 12i\pi G(1, x_2, 0, w) \\
& + 3i\pi G(1, x_2, 1, w) - 18G(1, 0, 0, -1, w) - 9G(1, 0, 0, 1, w) + 3G(1, 0, 1, 0, w) \\
& + 18G(1, x_1, 0, -1, w) - 12G(1, x_1, 0, 0, w) + 9G(1, x_1, 0, 1, w) - 3G(1, x_1, 1, 0, w) \\
& \left. \left. + 18G(1, x_2, 0, -1, w) - 12G(1, x_2, 0, 0, w) + 9G(1, x_2, 0, 1, w) - 3G(1, x_2, 1, 0, w) \right] \right. \\
& - \frac{2 (32w^5 - 19w^4 + 273w^3 - 177w^2 + 67w + 16)}{27 (w - 1)^2 (w + 1)} \left[8\pi^2 G(0, x_1, w) + 8\pi^2 G(0, x_2, w) \right. \\
& + 12i\pi G(0, x_1, 0, w) + 3i\pi G(0, x_1, 1, w) + 12i\pi G(0, x_2, 0, w) + 3i\pi G(0, x_2, 1, w) \\
& + 18G(0, x_1, 0, -1, w) - 12G(0, x_1, 0, 0, w) + 9G(0, x_1, 0, 1, w) - 3G(0, x_1, 1, 0, w) \\
& \left. \left. + 18G(0, x_2, 0, -1, w) - 12G(0, x_2, 0, 0, w) + 9G(0, x_2, 0, 1, w) - 3G(0, x_2, 1, 0, w) \right] \right. \\
& + \frac{4 (w^2 + 1)^2}{9 (w - 1)^2} \left[100i\pi G(0, -1, -1, w) + 76i\pi G(0, -1, 1, w) + 76i\pi G(0, 1, -1, w) \right. \\
& + 35i\pi G(0, 1, 1, w) - 100G(0, -1, -1, 0, w) - 28G(0, -1, 0, -1, w) - 14G(0, -1, 0, 1, w) \\
& - 76G(0, -1, 1, 0, w) + 128G(0, 0, -1, -1, w) + 64G(0, 0, -1, 1, w) + 64G(0, 0, 1, -1, w) \\
& + 32G(0, 0, 1, 1, w) - 76G(0, 1, -1, 0, w) + 4G(0, 1, 0, -1, w) + 2G(0, 1, 0, 1, w) \\
& \left. - 35G(0, 1, 1, 0, w) \right] - \frac{2w (24w^5 - 55w^4 + 300w^3 - 498w^2 + 276w - 55)}{9 (w - 1)^3 (w + 1)} \\
& \times \left[2G(0, 0, 0, -1, w) + G(0, 0, 0, 1, w) \right]
\end{aligned}$$

$$\begin{aligned}
& + \frac{w(6w^5 - w^4 + 8w^3 - 20w^2 + 2w - 1)}{9(w-1)^3(w+1)} \left[G(0, 0, 0, 0, w) - i\pi G(0, 0, 0, w) \right] \\
& + \frac{4(w^4 + 2w^3 + 4w^2 + 2w + 1)}{27(w^2 - 1)} \left[5\pi^2 G(1, 0, w) + 6i\pi G(1, 0, 0, w) - 6G(1, 0, 0, 0, w) \right] \\
& + \frac{8(24w^6 + 53w^5 - 314w^4 + 466w^3 - 306w^2 + 53w + 32)}{9(w-1)^3(w+1)} \\
& \times \left[G(0, 0, -1, 0, w) - i\pi G(0, 0, -1, w) \right] \\
& + \frac{2(29w^6 - 316w^5 + 1873w^4 - 2788w^3 + 1663w^2 - 316w - 181)}{9(w-1)^3(w+1)} \\
& \times \left[G(0, 1, 0, 0, w) - i\pi G(0, 1, 0, w) \right] \\
& + \frac{4(47w^6 + 79w^5 - 476w^4 + 693w^3 - 467w^2 + 79w + 56)}{9(w-1)^3(w+1)} \\
& \times \left[G(0, 0, 1, 0, w) - i\pi G(0, 0, 1, w) \right] \\
& + \frac{4(90w^6 - 313w^5 + 1820w^4 - 2776w^3 + 1602w^2 - 313w - 128)}{9(w-1)^3(w+1)} \\
& \times \left[G(0, -1, 0, 0, w) - i\pi G(0, -1, 0, w) \right] \\
& - \frac{2\pi^2(361w^6 - 1251w^5 + 7279w^4 - 11100w^3 + 6407w^2 - 1251w - 511) G(0, -1, w)}{27(w-1)^3(w+1)} \\
& - \frac{2\pi^2 w(8w^5 - w^4 + 10w^3 - 24w^2 + 2w - 1) G(0, 0, w)}{27(w-1)^3(w+1)} \\
& - \frac{2\pi^2(19w^6 - 211w^5 + 1249w^4 - 1860w^3 + 1109w^2 - 211w - 121) G(0, 1, w)}{9(w-1)^3(w+1)} \\
& - \frac{4}{9(w^2 - 1)} \left[3(8w^4 - 35w^3 + 190w^2 - 35w + 8) \zeta(3) \right. \\
& \left. + i\pi^3(w^4 + 2w^3 + 4w^2 + 2w + 1) \right] G(1, w) \\
& - \frac{1}{27(w-1)^3(w+1)} \left[6(15w^6 + w^5 + 13w^4 - 20w^3 - 3w^2 + w - 1) \zeta(3) \right. \\
& \left. - i\pi^3 w(10w^5 - w^4 + 12w^3 - 28w^2 + 2w - 1) \right] G(0, w) \\
& + \frac{\pi^4(231w^6 - 51w^5 + 333w^4 - 908w^3 + 121w^2 - 51w + 19)}{1620(w-1)^3(w+1)} \\
& + \frac{2i\pi(15w^6 + w^5 + 13w^4 - 20w^3 - 3w^2 + w - 1) \zeta(3)}{9(w-1)^3(w+1)} \\
& + \frac{4w^2}{135(w^2 - 1)} \left[900\zeta(3)G(0, w) - 30i\pi^3 G(0, w) + 180i\pi^3 G(1, w) - 360\pi^2 G(0, -1, w) \right. \\
& + 30\pi^2 G(0, 0, w) - 1080\pi^2 G(0, 1, w) - 300\pi^2 G(1, 0, w) - 720i\pi G(0, -1, 0, w) \\
& + 1440i\pi G(0, 0, -1, w) + 1080i\pi G(0, 0, 1, w) - 1440i\pi G(0, 1, 0, w) - 360i\pi G(1, 0, 0, w) \\
& \left. + 720G(0, -1, 0, 0, w) - 1440G(0, 0, -1, 0, w) - 1080G(0, 0, 1, 0, w) + 1440G(0, 1, 0, 0, w) \right]
\end{aligned}$$

$$+ 360G(1, 0, 0, 0, w) - 900i\pi\zeta(3) + 7\pi^4 \Big] + \dots, \quad (4.3)$$

where the color factors $C_F = 4/3$, $C_A = 3$, $T_R = 1/2$ have been substituted. The omitted terms have transcendental *weight* lower than four. The results for the other combinations of electroweak boson propagators are related to the above result by

$$X_{2,Vt\bar{t}}^{\gamma\gamma} = X_{2,Vt\bar{t}}^{\gamma Z} = X_{2,Vt\bar{t}}^{ZZ} \Big|_{c_{\text{axi}}=0}. \quad (4.4)$$

The contribution from the four top (anti-)quarks contains master integrals depending on elliptic integrals. It was found that one can choose such a regular basis that only the $\mathcal{O}(\epsilon^0)$ parts of the master integrals are required [51]. The regular basis consists of twelve integrals $F_i^{4t}(z)$, $i = 1, \dots, 12$, that can be expressed either as complete elliptic integrals of the first kind or one-fold integrals of them. Their explicit definitions are given in the appendix of [51]. Based on this basis, we give the result of four top quark production,

$$\begin{aligned} X_{2,Vt\bar{t}}^{ZZ,4t} = & \frac{c_{\text{vec,u}}^2}{(c_{\text{axi}}^2(z-4) + c_{\text{vec,u}}^2(z+2))} \left(\frac{F_1^{4t}(z)(3z^2 + 430z + 128)}{10368\pi r_1} \right. \\ & + \frac{F_2^{4t}(z)(85z^3 + 990z^2 + 16680z - 92608)}{15552\pi r_1(z-4)} - \frac{F_3^{4t}(z)(1019z^2 - 1286z - 12120)}{3888\pi r_1} \\ & - \frac{F_4^{4t}(z)(z-6)(49z^2 - 336z + 464)}{1296\pi(z-4)^2} - \frac{F_5^{4t}(z)(z-1)(z+2)}{108\pi r_1} \\ & - \frac{F_6^{4t}(z)(z)(z^2 + 2z - 18)}{54\pi(z-4)} + \frac{F_7^{4t}(z)(5z^2 - 12z - 50)}{216\pi r_1} \\ & + \frac{F_8^{4t}(z)(5z^2 - 2z - 60)}{108\pi(z-4)} + \frac{F_9^{4t}(z)(z^2 + z + 4)}{108\pi r_1} \\ & \left. + \frac{F_{10}^{4t}(z)(z^2 - 2)}{54\pi r_1} - \frac{F_{12}^{4t}(z)(z+2)(z-2)^2}{54\pi(z-4)z} \right) \\ & + \frac{c_{\text{axi}}^2}{(c_{\text{axi}}^2(z-4) + c_{\text{vec,u}}^2(z+2))} \left(- \frac{F_1^{4t}(z)(114z^2 + 2189z + 2140)}{10368\pi r_1} \right. \\ & + \frac{F_2^{4t}(z)(490z^3 + 5821z^2 - 21476z + 20256)}{15552\pi r_1 z} - \frac{F_3^{4t}(z)r_1(1424z^2 - 2235z + 2532)}{3888\pi z^2} \\ & - \frac{F_4^{4t}(z)(85z^3 - 980z^2 + 2076z + 1296)}{1296\pi(z-4)z} - \frac{F_5^{4t}(z)(4z^2 - 11z + 16)}{432\pi r_1} \\ & - \frac{F_6^{4t}(z)(4z^2 - 55z + 6)}{216\pi z} + \frac{F_7^{4t}(z)(5z^3 - 18z^2 + 2z + 84)}{216\pi r_1 z} \\ & + \frac{F_8^{4t}(z)(10z^2 - 79z + 6)}{216\pi z} + \frac{F_9^{4t}(z)(z^3 - 7z^2 - 36z - 6)}{108\pi r_1 z} \\ & \left. + \frac{F_{10}^{4t}(z)(z^2 - 6z - 2)}{54\pi r_1} - \frac{F_{12}^{4t}(z)(z-2)^2}{54\pi z} \right), \quad (4.5) \end{aligned}$$

where the color factors $C_F = 4/3$, $C_A = 3$ have been substituted. The results for the other

electroweak boson combinations are given by

$$X_{2,Vt\bar{t}}^{\gamma\gamma,4t} = X_{2,Vt\bar{t}}^{\gamma Z,4t} = X_{2,Vt\bar{t}}^{ZZ,4t} \Big|_{c_{\text{axi}}=0}. \quad (4.6)$$

We have compared with [51] for the result of $X_{2,Vt\bar{t}}^{\gamma\gamma,4t}$ and found full agreement ¹.

The full result of $X_{2,gt\bar{t}}$ can be written as

$$X_{2,gt\bar{t}}^{VV'} = C_F F_{2,gt\bar{t}}^{VV'} \tilde{X}_{2,gt\bar{t}} \quad (4.7)$$

with

$$\begin{aligned} F_{2,gt\bar{t}}^{\gamma\gamma} &= -\frac{e_d^2 n_{l,d} + e_u^2 n_{l,u}}{(z+2)e_u^2}, \\ F_{2,gt\bar{t}}^{\gamma Z} &= -\frac{c_{\text{vec,u}} e_u n_{l,u} + c_{\text{vec,d}} e_d n_{l,d}}{(z+2)c_{\text{vec,u}} e_u}, \\ F_{2,gt\bar{t}}^{ZZ} &= -\frac{c_{\text{axi}}^2 n_l + c_{\text{vec,d}}^2 n_{l,d} + c_{\text{vec,u}}^2 n_{l,u}}{c_{\text{axi}}^2 (z-4) + c_{\text{vec,u}}^2 (z+2)}. \end{aligned} \quad (4.8)$$

Here e_u (e_d) and $n_{l,u}$ ($n_{l,d}$) stand for the charge and number of light up-type (down-type) quarks, respectively, and $n_l = n_{l,u} + n_{l,d}$. It can be seen that

$$F_{2,gt\bar{t}}^{\gamma\gamma} = F_{2,gt\bar{t}}^{\gamma Z} = F_{2,gt\bar{t}}^{ZZ} \text{ if } c_{\text{axi}} = 0 \text{ and } \frac{c_{\text{vec,u}}}{c_{\text{vec,d}}} = \frac{e_u}{e_d}. \quad (4.9)$$

The complete form of $\tilde{X}_{2,gt\bar{t}}$ reads

$$\begin{aligned} \tilde{X}_{2,gt\bar{t}} &= \frac{(r_1 - z)}{r_1 - z + 4} \left(-\frac{z^2 - 6}{18z} \left[2\pi^2 G(-1, y) - \pi^2 G(0, y) - \pi^2 G(1, y) - \pi^2 G(-i, y) \right. \right. \\ &\quad - \pi^2 G(i, y) + 3G(-1, -1, -1, y) + 3G(-1, -1, 0, y) - 3G(-1, -1, 1, y) \\ &\quad - 9G(-1, 0, -1, y) - 9G(-1, 0, 0, y) + 9G(-1, 0, 1, y) - 9G(-1, 1, -1, y) \\ &\quad - 9G(-1, 1, 0, y) + 9G(-1, 1, 1, y) + 6G(-1, -i, -1, y) + 6G(-1, -i, 0, y) \\ &\quad - 6G(-1, -i, 1, y) + 6G(-1, i, -1, y) + 6G(-1, i, 0, y) - 6G(-1, i, 1, y) \\ &\quad - 9G(0, -1, -1, y) - 9G(0, -1, 0, y) + 9G(0, -1, 1, y) + 3G(0, 0, -1, y) \\ &\quad + 3G(0, 0, 0, y) - 3G(0, 0, 1, y) + 3G(0, 1, -1, y) + 3G(0, 1, 0, y) - 3G(0, 1, 1, y) \\ &\quad + 6G(0, -i, -1, y) + 6G(0, -i, 0, y) - 6G(0, -i, 1, y) + 6G(0, i, -1, y) + 6G(0, i, 0, y) \\ &\quad - 6G(0, i, 1, y) - 9G(1, -1, -1, y) - 9G(1, -1, 0, y) + 9G(1, -1, 1, y) + 3G(1, 0, -1, y) \\ &\quad + 3G(1, 0, 0, y) - 3G(1, 0, 1, y) + 3G(1, 1, -1, y) + 3G(1, 1, 0, y) - 3G(1, 1, 1, y) \\ &\quad + 6G(1, -i, -1, y) + 6G(1, -i, 0, y) - 6G(1, -i, 1, y) + 6G(1, i, -1, y) + 6G(1, i, 0, y) \\ &\quad - 6G(1, i, 1, y) + 6G(-i, -1, -1, y) + 6G(-i, -1, 0, y) - 6G(-i, -1, 1, y) \\ &\quad + 6G(-i, 0, -1, y) + 6G(-i, 0, 0, y) - 6G(-i, 0, 1, y) + 6G(-i, 1, -1, y) + 6G(-i, 1, 0, y) \\ &\quad \left. - 6G(-i, 1, 1, y) - 12G(-i, -i, -1, y) - 12G(-i, -i, 0, y) + 12G(-i, -i, 1, y) \right] \end{aligned}$$

¹There is a typo in eq. (4.6) of [51], e.g., the denominator 5s should be changed to 2s.

$$\begin{aligned}
& -12G(-i, i, -1, y) - 12G(-i, i, 0, y) + 12G(-i, i, 1, y) + 6G(i, -1, -1, y) \\
& + 6G(i, -1, 0, y) - 6G(i, -1, 1, y) + 6G(i, 0, -1, y) + 6G(i, 0, 0, y) - 6G(i, 0, 1, y) \\
& + 6G(i, 1, -1, y) + 6G(i, 1, 0, y) - 6G(i, 1, 1, y) - 12G(i, -i, -1, y) - 12G(i, -i, 0, y) \\
& + 12G(i, -i, 1, y) - 12G(i, i, -1, y) - 12G(i, i, 0, y) + 12G(i, i, 1, y) \Big] \\
& + \frac{(z+4)(19z+46)}{18r_2} \left[G(-1, -1, y) + G(-1, 0, y) - G(-1, 1, y) - G(0, -1, y) \right. \\
& \left. - G(0, 0, y) + G(0, 1, y) - G(1, -1, y) - G(1, 0, y) + G(1, 1, y) \right] \\
& - \frac{(19z^2 + 72z + 72)}{108z} \left[3i\pi G(0, w) - 6i\pi G(1, w) - 3G(0, 0, w) + 6G(1, 0, w) + 2\pi^2 \right] \\
& - \frac{(73z^2 + 222z + 189)}{54z} \left[G(0, w) - i\pi \right] - \frac{2(z-4)(2123z + 4978)}{1296r_1} \\
& + \frac{\pi^2 (19z^2 + 122z + 184)}{72r_2} + \frac{5(z^2 - 6)\zeta(3)}{6z} \Big). \tag{4.10}
\end{aligned}$$

5 Asymptotic expansion

With the full analytic results at hand, it is interesting to investigate the asymptotic expansions in some limits.

We first consider the threshold limit when the quark velocity $\beta = \sqrt{1 - 4/z}$ is small. The QCD NLO corrections near the threshold are

$$\begin{aligned}
X_{1, V\bar{t}t}^{ZZ}|_{\beta \rightarrow 0} &= \frac{c_{\text{vec,u}}^2(z+2)C_F}{(c_{\text{axi}}^2(z-4) + c_{\text{vec,u}}^2(z+2))} \left(\frac{\pi^2}{2\beta} - 4 + \frac{\pi^2\beta}{2} + \mathcal{O}(\beta^2) \right) \\
&+ \frac{c_{\text{axi}}^2(z-4)C_F}{(c_{\text{axi}}^2(z-4) + c_{\text{vec,u}}^2(z+2))} \left(\frac{\pi^2}{2\beta} - 2 + \frac{\pi^2\beta}{2} + \mathcal{O}(\beta^2) \right). \tag{5.1}
\end{aligned}$$

As in the full result, $X_{1, V\bar{t}t}^{\gamma\gamma}|_{\beta \rightarrow 0}$ and $X_{1, V\bar{t}t}^{\gamma Z}|_{\beta \rightarrow 0}$ can be obtained from $X_{1, V\bar{t}t}^{ZZ}|_{\beta \rightarrow 0}$ by setting $c_{\text{axi}} = 0$. Notice that we do not expand the prefactors in $X_{1, V\bar{t}t}^{ZZ}|_{\beta \rightarrow 0}$. They arise because the corrections are compared to the LO result which contains

$$c_{\text{axi}}^2(z-4) + c_{\text{vec,u}}^2(z+2) = \frac{-4c_{\text{axi}}^2\beta^2 + 2(\beta^2 - 3)c_{\text{vec,u}}^2}{\beta^2 - 1}. \tag{5.2}$$

It is observed that the axial-vector current gives a contribution suppressed by β^2 relative to the vector current.

With the help of the `PolyLogTools` package [52] and the relations among MPLs in [53, 54], the QCD NNLO corrections near the threshold can be expanded as

$$\begin{aligned}
X_{2, V\bar{t}t}^{ZZ}|_{\beta \rightarrow 0} &= \frac{c_{\text{vec,u}}^2(z+2)}{(c_{\text{axi}}^2(z-4) + c_{\text{vec,u}}^2(z+2))} \left(C_F^2 \left[\frac{\pi^4}{12\beta^2} - \frac{2\pi^2}{\beta} - \frac{2\pi^2 \log(\beta)}{3} + \frac{\pi^4}{6} \right. \right. \\
&+ \frac{4\pi^2 \log(2)}{3} - \zeta(3) - \frac{35\pi^2}{18} + \frac{39}{4} + \frac{8\pi^2 \log(\beta)}{3} \beta + \frac{4\pi^2 \log(2)}{3} \beta - \frac{55\pi^2}{18} \beta + \mathcal{O}(\beta^2) \Big] \\
&+ C_A C_F \left[-\frac{11\pi^2 \log(\beta)}{12\beta} + \frac{11\pi^2}{24\beta} \log\left(\frac{\mu^2}{s}\right) + \frac{31\pi^2}{72\beta} - \pi^2 \log(\beta) - \frac{11}{3} \log\left(\frac{4\mu^2}{s}\right) \right]
\end{aligned}$$

$$\begin{aligned}
& -\frac{8\pi^2 \log(2)}{3} - \frac{13\zeta(3)}{2} + \frac{179\pi^2}{72} - \frac{151}{36} - \frac{\pi^2}{4}\beta \log(\beta) + \frac{11\pi^2}{24}\beta \log\left(\frac{\mu^2}{s}\right) \\
& + \frac{8\pi^2 \log(2)\beta}{3} + \frac{193\pi^2\beta}{72} + \mathcal{O}(\beta^2) \Big] \\
& + C_{Fn_l} \left[\frac{\pi^2 \log(\beta)}{6\beta} - \frac{\pi^2}{12\beta} \log\left(\frac{\mu^2}{s}\right) - \frac{5\pi^2}{36\beta} + \frac{2}{3} \log\left(\frac{4\mu^2}{s}\right) + \frac{11}{18} + \frac{\pi^2\beta \log(\beta)}{6} \right. \\
& - \left. \frac{\pi^2}{12}\beta \log\left(\frac{\mu^2}{s}\right) - \frac{13\pi^2\beta}{36} + \mathcal{O}(\beta^2) \right] \\
& + C_F \left[-\frac{\pi^2}{12\beta} \log\left(\frac{4\mu^2}{s}\right) + \frac{2}{3} \log\left(\frac{4\mu^2}{s}\right) - \frac{2\pi^2}{9} + \frac{22}{9} - \frac{\pi^2}{12}\beta \log\left(\frac{4\mu^2}{s}\right) \right. \\
& - \left. \frac{\pi^2\beta}{12} + \mathcal{O}(\beta^2) \right] \Big) \\
& + \frac{c_{\text{axi}}^2(z-4)}{(c_{\text{axi}}^2(z-4) + c_{\text{vec,u}}^2(z+2))} \left(C_F^2 \left[\frac{\pi^4}{12\beta^2} + \frac{\pi^2}{4\beta^2} - \frac{\pi^2}{\beta} - \frac{5\pi^2}{6} \log(\beta) + \frac{\pi^4}{6} \right. \right. \\
& + \left. \left. \frac{3\pi^2 \log(2)}{4} - \frac{27\zeta(3)}{8} + \frac{\pi^2}{12} + \frac{35}{12} + \frac{8\pi^2}{3}\beta \log(\beta) + \frac{4\pi^2 \log(2)\beta}{3} - \frac{32\pi^2}{9}\beta + \mathcal{O}(\beta^2) \right] \right. \\
& + C_A C_F \left[-\frac{11\pi^2 \log(\beta)}{12\beta} + \frac{11\pi^2}{24\beta} \log\left(\frac{\mu^2}{s}\right) + \frac{97\pi^2}{72\beta} - \frac{\pi^2 \log(\beta)}{3} - \frac{11}{6} \log\left(\frac{4\mu^2}{s}\right) \right. \\
& - \left. \frac{3\pi^2 \log(2)}{2} - \frac{9\zeta(3)}{4} + \frac{89\pi^2}{72} - \frac{101}{36} - \frac{\pi^2\beta \log(\beta)}{4} + \frac{11}{24}\pi^2\beta \log\left(\frac{\mu^2}{s}\right) \right. \\
& + \left. \frac{37\pi^2\beta}{24} + \frac{8\pi^2 \log(2)\beta}{3} + \mathcal{O}(\beta^2) \right] \\
& + C_{Fn_l} \left[\frac{\pi^2 \log(\beta)}{6\beta} - \frac{\pi^2}{12\beta} \log\left(\frac{\mu^2}{s}\right) - \frac{11\pi^2}{36\beta} + \frac{1}{3} \log\left(\frac{4\mu^2}{s}\right) + \frac{7}{18} \right. \\
& + \left. \frac{\pi^2\beta \log(\beta)}{6} - \frac{\pi^2\beta}{12} \log\left(\frac{\mu^2}{s}\right) - \frac{2\pi^2\beta}{9} + \mathcal{O}(\beta^2) \right] \\
& + C_F \left[-\frac{\pi^2}{12\beta} \log\left(\frac{4\mu^2}{s}\right) + \frac{1}{3} \log\left(\frac{\mu^2}{s}\right) - \frac{13\pi^2}{24} + \frac{2\log^2(2)}{3} + \frac{2\pi^2 \log(2)}{3} \right. \\
& - \left. \frac{4\log(2)}{3} + \frac{20}{9} - \frac{\pi^2}{12}\beta \log\left(\frac{4\mu^2}{s}\right) - \frac{\pi^2\beta}{12} + \mathcal{O}(\beta^2) \right] \Big). \tag{5.3}
\end{aligned}$$

We have compared the expression of $X_{2,V\bar{t}\bar{t}}^{ZZ}|_{\beta \rightarrow 0}$ with the two-loop virtual corrections near the threshold [10, 55–57], finding full agreement for the terms up to $\mathcal{O}(\beta^0)$.

The fixed-order predictions for the cross sections near the threshold are not valid anymore because the contributions from the $1/\beta^2$ terms become divergent. These terms are induced by the color Coulomb interaction between the final-state heavy quarks. The resummation of the leading divergent terms of the form α_s^n/β^n gives rise to the well-known Sommerfeld-Sakharov factor. The subleading divergent terms α_s^{n+1}/β^n can also be resummed to all orders by calculating the Coulomb Green function. See, e.g., refs. [13] and [58] for the S- and P-wave contributions, respectively.

We remark that the contribution from the diagrams in which the top quarks do not

couple to the electroweak boson directly is strongly suppressed near the threshold,

$$\tilde{X}_{2,g\bar{t}\bar{t}}|_{\beta \rightarrow 0} = -\frac{128}{45045}\beta^{12} + \mathcal{O}(\beta^{13}). \quad (5.4)$$

Therefore, it is reasonable to neglect this contribution near the threshold.

Then we consider the limit of $z \rightarrow \infty$, which corresponds to taking the massless limit of the quark mass. The QCD NLO corrections are expanded in this limit as

$$\begin{aligned} X_{1,V\bar{t}\bar{t}}^{ZZ}|_{z \rightarrow \infty} &= \frac{c_{\text{vec,u}}^2(z+2)C_F}{(c_{\text{axi}}^2(z-4) + c_{\text{vec,u}}^2(z+2))} \left(\frac{3}{4} + \frac{9}{z} + \mathcal{O}\left(\frac{1}{z^2}\right) \right) \\ &+ \frac{c_{\text{axi}}^2(z-4)C_F}{(c_{\text{axi}}^2(z-4) + c_{\text{vec,u}}^2(z+2))} \left(\frac{3}{4} + \frac{9\log(z)}{z} + \mathcal{O}\left(\frac{1}{z^2}\right) \right), \end{aligned} \quad (5.5)$$

and

$$X_{1,V\bar{t}\bar{t}}^{\gamma\gamma}|_{z \rightarrow \infty} = X_{1,V\bar{t}\bar{t}}^{\gamma Z}|_{z \rightarrow \infty} = C_F \left(\frac{3}{4} + \frac{9}{z} + \mathcal{O}\left(\frac{1}{z^2}\right) \right). \quad (5.6)$$

We see that the limit can be taken continuously, though there is a logarithmic enhancement at subleading power in the axial-vector coupling case.

At NNLO, the contributions from two and four top quark final states are singular individually, i.e., they are divergent as $z \rightarrow \infty$. This is due to the infrared divergences in the massless limit. A similar behavior has been observed in $H \rightarrow b\bar{b}$ [39]. However, their sum is finite in this limit, and is given by

$$\begin{aligned} (X_{2,V\bar{t}\bar{t}}^{ZZ} + X_{2,V\bar{t}\bar{t}}^{ZZ,4t})|_{z \rightarrow \infty} &= \frac{c_{\text{vec,u}}^2(z+2)}{(c_{\text{axi}}^2(z-4) + c_{\text{vec,u}}^2(z+2))} \times \\ &\left(C_F^2 \left[-\frac{3}{32} - \frac{27\log(z)}{2z} + \frac{9}{8z} + \mathcal{O}\left(\frac{1}{z^2}\right) \right] \right. \\ &+ C_A C_F \left[\frac{11}{16} \log\left(\frac{\mu^2}{s}\right) + \frac{123}{32} - \frac{11\zeta(3)}{4} + \frac{33}{4z} \log\left(\frac{\mu^2}{s}\right) + \frac{185}{8z} + \mathcal{O}\left(\frac{1}{z^2}\right) \right] \\ &+ C_F n_l \left[-\frac{1}{8} \log\left(\frac{\mu^2}{s}\right) + \frac{\zeta(3)}{2} - \frac{11}{16} - \frac{3}{2z} \log\left(\frac{\mu^2}{s}\right) - \frac{13}{4z} + \mathcal{O}\left(\frac{1}{z^2}\right) \right] \\ &\left. + C_F \left[-\frac{1}{8} \log\left(\frac{\mu^2}{s}\right) + \frac{\zeta(3)}{2} - \frac{11}{16} - \frac{3}{2z} \log\left(\frac{\mu^2}{s}\right) - \frac{13}{4z} + \mathcal{O}\left(\frac{1}{z^2}\right) \right] \right) \\ &+ \frac{c_{\text{axi}}^2(z-4)}{(c_{\text{axi}}^2(z-4) + c_{\text{vec,u}}^2(z+2))} \times \\ &\left(C_F^2 \left[-\frac{3}{32} - \frac{27\log^2(z)}{4z} + \frac{63\log(z)}{8z} - \frac{6\pi^2\log(2)}{z} + \frac{45\zeta(3)}{2z} + \frac{6\pi^2}{z} - \frac{195}{8z} + \mathcal{O}\left(\frac{1}{z^2}\right) \right] \right. \\ &+ C_A C_F \left[\frac{11}{16} \log\left(\frac{\mu^2}{s}\right) - \frac{11\zeta(3)}{4} + \frac{123}{32} + \frac{33\log^2(z)}{8z} + \frac{185\log(z)}{8z} + \frac{33}{4z} \log(z) \log\left(\frac{\mu^2}{s}\right) \right. \\ &\left. + \frac{3\pi^2\log(2)}{z} + \frac{9\zeta(3)}{4z} + \frac{3\pi^2}{8z} - \frac{89}{16z} + \mathcal{O}\left(\frac{1}{z^2}\right) \right] \\ &\left. + C_F n_l \left[-\frac{1}{8} \log\left(\frac{\mu^2}{s}\right) + \frac{\zeta(3)}{2} - \frac{11}{16} - \frac{3\log^2(z)}{4z} - \frac{3\log(z)}{2z} \log\left(\frac{\mu^2}{s}\right) \right] \right) \end{aligned}$$

$$\begin{aligned}
& -\frac{13\log(z)}{4z} - \frac{3\pi^2}{4z} + \frac{7}{8z} + \mathcal{O}\left(\frac{1}{z^2}\right) \Big] \\
& + C_F \left[-\frac{1}{8} \log\left(\frac{\mu^2}{s}\right) + \frac{\zeta(3)}{2} - \frac{\pi^2}{12} + \frac{1}{4} - \frac{5\log^2(z)}{4z} - \frac{3\log(z)}{2z} \log\left(\frac{\mu^2}{s}\right) \right. \\
& \left. - \frac{25\log(z)}{4z} + \frac{13\pi^2}{12z} + \frac{1}{z} + \mathcal{O}\left(\frac{1}{z^2}\right) \right] \Big]. \tag{5.7}
\end{aligned}$$

Again, the results for the $\gamma\gamma$ and γZ combinations can be obtained by setting $c_{\text{axi}} = 0$. The contribution in this limit agrees with the results given in refs. [19–21].

Finally, the contribution of the processes in which the top quark pair is produced from a gluon is singular and has the following expansion form.

$$\begin{aligned}
& \tilde{X}_{2,g\bar{t}t}|_{z \rightarrow \infty} \\
& = -\frac{z\log^3(z)}{36} + \frac{19z\log^2(z)}{72} + \frac{\pi^2 z\log(z)}{18} - \frac{73z\log(z)}{54} - \frac{5\zeta(3)z}{6} - \frac{19\pi^2 z}{108} + \frac{2123z}{648} \\
& - \frac{\log^3(z)}{18} + \frac{55\log^2(z)}{36} + \frac{\pi^2 \log(z)}{9} - \frac{127\log(z)}{27} - \frac{5\zeta(3)}{3} - \frac{55\pi^2}{54} + \frac{4715}{324} + \mathcal{O}\left(\frac{1}{z^2}\right). \tag{5.8}
\end{aligned}$$

This singular structure indicates that the cross section for a quark pair production with a specific flavor is sensitive to infrared effects, e.g., a gluon splitting to such a collinear quark pair. Since the specific quark cannot be distinguished from the other massless quarks in this limit, it would be difficult to measure such a process with physical detectors. A more realistic observable is the jet cross section which includes contributions from both the specific quark and other partons. In this case, it is necessary to consider the diagrams with a top quark loop in the virtual gluon propagator. Their contribution would cancel against the large logarithmic terms in eq.(5.8), giving rise to a finite result in the $z \rightarrow \infty$ limit.

6 Numerical results

With the analytical results at hand, it is ready to present their numerical impact in phenomenological studies. We take the numerical inputs as in ref. [28],

$$\begin{aligned}
& m_W = 80.385 \text{ GeV}, \quad m_Z = 91.1876 \text{ GeV}, \quad m_t = 172.69 \text{ GeV}, \\
& \alpha = \frac{1}{132.2}, \quad \alpha_s(m_Z) = 0.1181, \quad \Gamma_Z = 2.4952 \text{ GeV}, \tag{6.1}
\end{aligned}$$

and $\cos\theta_W = m_W/m_Z$. The package RunDec [59, 60] was used to calculate α_s at other scales. First, we present the numerical values for the perturbative expansion coefficients at different orders in table 1. From the LO results, one can see that $\sigma^{\gamma\gamma}$ is the dominant contribution to the $e^-e^+ \rightarrow t\bar{t}$ process. The NLO coefficients, $X_1^{\gamma\gamma}$ and X_1^{ZZ} , decrease with the increasing of the collision energy. Because of the axial current contribution, the corrections induced by a Z boson exchange are larger than those by a photon. The NNLO coefficients $X_{2,V\bar{t}t}^{\gamma\gamma}$ and $X_{2,V\bar{t}t}^{ZZ}$ exhibit similar features. Moreover, it is interesting to note the large magnitude of these coefficients at $\sqrt{s} = 350$ GeV. Even multiplied by the expansion

| \sqrt{s} | 350 GeV | 500 GeV | 1000 GeV |
|--|-------------------------------|------------------------------|------------------------------|
| $\sigma_{\text{LO}}^{\gamma\gamma}$ (pb) | 2.4459×10^{-1} | 4.4577×10^{-1} | 1.2374×10^{-1} |
| σ_{LO}^{ZZ} (pb) | 1.5198×10^{-2} | 8.2932×10^{-2} | 3.7130×10^{-2} |
| $\sigma_{\text{LO}}^{\gamma Z}$ (pb) | 1.2490×10^{-2} | 2.1948×10^{-2} | 5.9393×10^{-3} |
| $X_1^{\gamma\gamma}$ | 35.87815637 | 3.902679560 | 1.454200325 |
| X_1^{ZZ} | 36.13473849 | 5.385227064 | 2.242695157 |
| $X_{2,Vt\bar{t}}^{\gamma\gamma}$ | 739.8408382 | 15.48165668 | 1.237511900 |
| $X_{2,Vt\bar{t}}^{ZZ}$ | 779.1581353 | 46.69192781 | 11.22389311 |
| $X_{2,Vt\bar{t}}^{ZZ,S}$ | $3.524878161 \times 10^{-2}$ | $-2.47153096 \times 10^{-1}$ | $-2.09396980 \times 10^{-1}$ |
| $X_{2,Vt\bar{t}}^{\gamma\gamma,4t}$ | 0 | 0 | $4.852649148 \times 10^{-3}$ |
| $X_{2,Vt\bar{t}}^{ZZ,4t}$ | 0 | 0 | $2.389195068 \times 10^{-3}$ |
| $X_{2,gt\bar{t}}^{\gamma\gamma}$ | $6.063662743 \times 10^{-13}$ | $2.166216155 \times 10^{-4}$ | $6.792148588 \times 10^{-2}$ |
| $X_{2,gt\bar{t}}^{\gamma Z}$ | $1.014082252 \times 10^{-13}$ | $3.622763087 \times 10^{-4}$ | $1.135913659 \times 10^{-1}$ |
| $X_{2,gt\bar{t}}^{ZZ}$ | $8.244429044 \times 10^{-12}$ | $9.145040414 \times 10^{-4}$ | $1.689525260 \times 10^{-1}$ |

Table 1: Numerical results for the perturbative expansion coefficients at different collision energies. $X_{2,Vt\bar{t}}^{ZZ,S}$ represents the contribution from the flavor singlet diagrams in $X_{2,Vt\bar{t}}^{ZZ}$. The renormalization scale is chosen as $\mu = \sqrt{s}$.

parameter $(\alpha_s/\pi)^i, i = 1, 2$, they provide corrections of about 100% to the LO result. Adopting the result with the Coulomb resummation is more appropriate in this threshold region as in [14, 61]. All of the numerical results in table 1 have been cross checked with those in [28] except for $X_{2,Vt\bar{t}}^{4t}$ and perfect agreements were found.

In $X_{2,Vt\bar{t}}^{ZZ}$, the contribution from flavour singlet diagrams is a special part that involves a quark loop. It turns out to be a small correction, only at most 2% of the total $X_{2,Vt\bar{t}}^{ZZ}$ at $\sqrt{s} = 1000$ GeV. The contributions of the four top quark final states or of the diagrams with a gluon splitting to two top quarks are also so tiny that they could be neglected in phenomenological studies.

Then we show the total cross sections of top quark pair production at different perturbative orders in figure 4. The cross section first increases and then decreases when the collider energy changes from 350 GeV to 1000 GeV. The peak positions move from 416 GeV at LO, to 392 GeV at NLO and 381 GeV at NNLO at $\mu = \sqrt{s}$. The higher-order QCD corrections are more significant for the process with smaller collision energies. At $\sqrt{s} = 400$ GeV, the NLO correction improves the LO cross section by 26%, and the NNLO correction provides additional 5% enhancement when choosing the renormalization scale $\mu = \sqrt{s}$. At $\sqrt{s} = 1000$ GeV, the NLO and NNLO corrections reduce to only 5% and 0.3%, respectively. It is also important to observe that the QCD renormalization scale uncertainty, which is

evaluated by varying the default scale $\mu = \sqrt{s}$ by a factor of two, is decreased from 3.2% (0.6%) at NLO to 1.6% (0.09%) at NNLO for collisions at $\sqrt{s} = 400$ (1000) GeV. Note that our results may not be valid near the top quark pair production threshold due to the reason discussed in the last section.

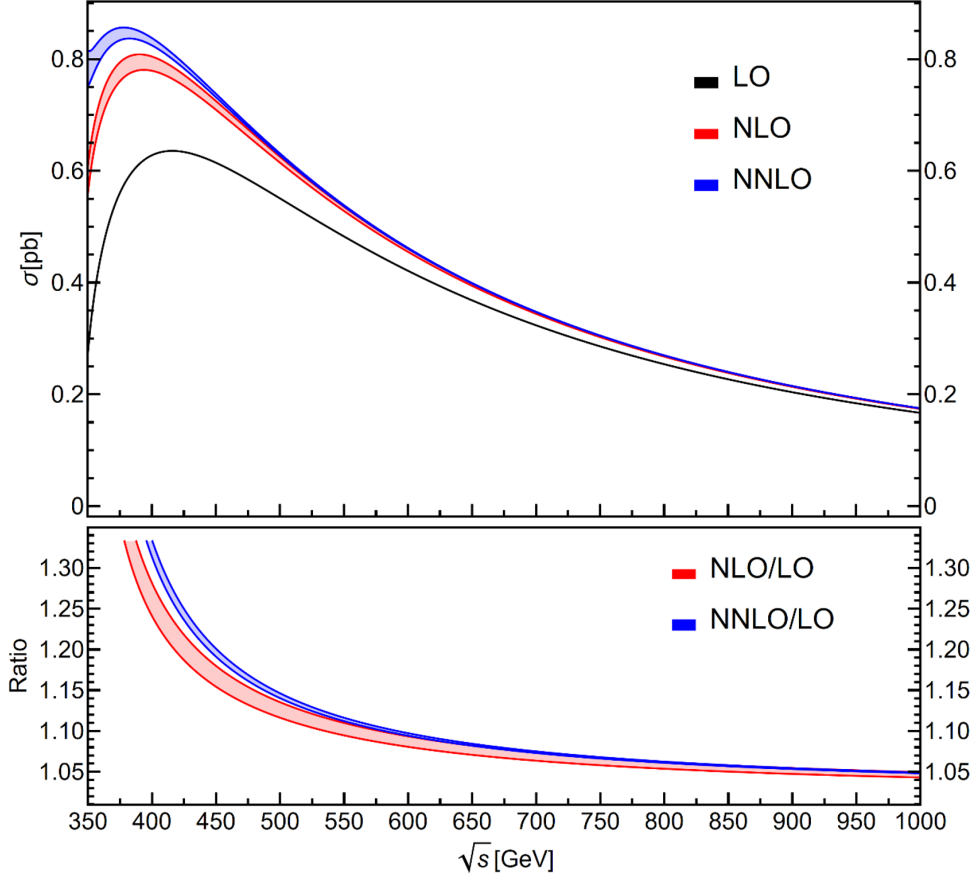


Figure 4: Numerical results for the total cross sections of top quark pair production. The bands denote the scale uncertainties with the scale $\mu \in [\sqrt{s}/2, 2\sqrt{s}]$. In the bottom plot, we show the ratios of higher-order results over the LO one.

We also provide the results in the $\overline{\text{MS}}$ renormalization scheme which are converted from the on-shell scheme with the mass relation in [62–65]. As shown in figure 5, the cross sections in the $\overline{\text{MS}}$ scheme exhibit much better convergence behavior. The reason is that the pole mass is by definition plagued by the renormalon problem [66]. When more perturbative corrections are included, the difference between the two renormalization schemes is notably reduced.

One of the motivations for studying top quark pair production at electron colliders is to investigate the coupling between the top quarks and the Z boson. We show the cross section induced by Z propagators $\sigma_{e^-e^+\rightarrow t\bar{t}}^{ZZ}$ in figure 6. We split the contributions into the vector and axial-vector quark currents. The axial-vector current contributions are strongly suppressed near the threshold; see eq.(5.2) above. With the increasing of the

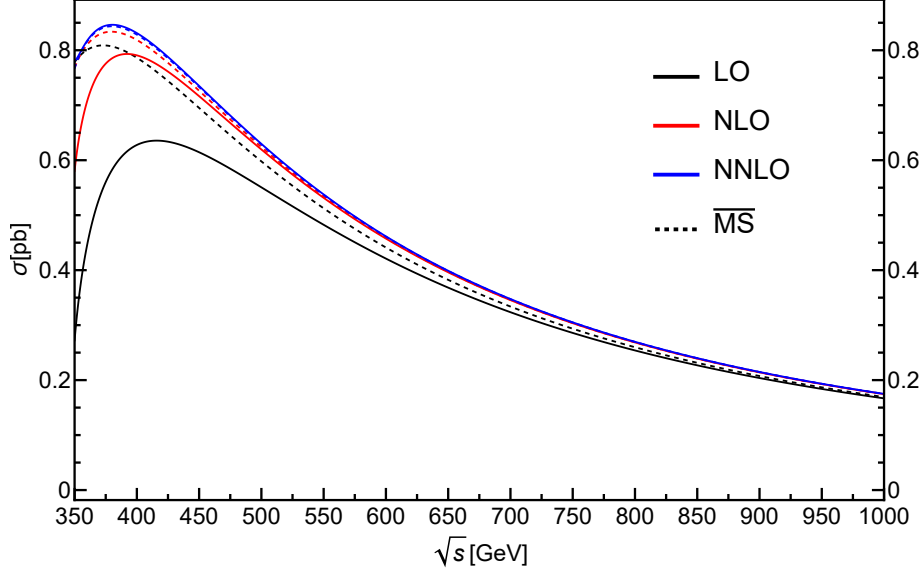


Figure 5: The cross sections in the on-shell (solid lines) and $\overline{\text{MS}}$ (dashed lines) renormalization schemes for the top quark mass. The renormalization scale $\mu = \sqrt{s}$ is used.

collision energy, the axial-vector contributions grow rapidly and become larger than the vector contributions when $\sqrt{s} > 400$ GeV. This is because the axial-vector current coupling c_{axi}^2 (≈ 0.08) is larger than the vector current coupling $c_{\text{vec,u}}^2$ (≈ 0.01). We also see that the QCD corrections in the axial-vector current contribution are more significant than those in the vector current.

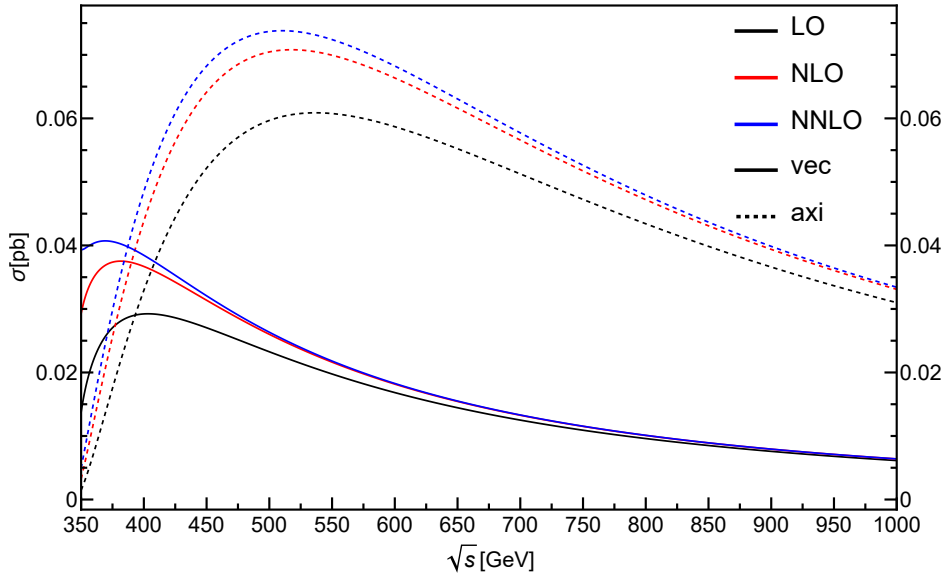


Figure 6: The cross section $\sigma_{e^-e^+ \rightarrow t\bar{t}}^{ZZ}$ as a function of \sqrt{s} . The renormalization scale is chosen at $\mu = \sqrt{s}$. The solid and dash lines represent the vector current and axial-vector current contributions in $\sigma_{e^-e^+ \rightarrow t\bar{t}}^{ZZ}$, respectively.

7 Conclusion

In this paper, we have presented the analytic results of NNLO QCD corrections to top quark pair production at lepton colliders. We consider the contributions from both a photon and a Z boson propagator. Part of the required master integrals are available in our previous paper on the $H \rightarrow bb$ decay, and the others are computed explicitly using the canonical differential equations. The full analytical NNLO QCD corrections are divided into the contributions of two and four top quark final states. The former is expressed in terms of multiple polylogarithms, while the latter is written as a linear combination of complete elliptic integrals and one-fold integrals of them. Near the threshold, the expansion up to $\mathcal{O}(\beta^0)$ agrees with the corresponding virtual corrections and are compatible with the prediction of the Coulomb resummation formula. In the high energy limit, the sum of the contributions from the two and four top quark final states is finite, though they are individually divergent. Numerically, the photon-induced process has a larger contribution to the total cross section than the Z boson-induced one. But the higher-order correction is more significant in the Z boson-induced process. At $\sqrt{s} = 400$ GeV, the NNLO corrections increase the NLO result by 5% and decrease the scale uncertainty by a factor of two. The QCD corrections become smaller at higher collision energies. We also find that the results in the $\overline{\text{MS}}$ top quark mass scheme show faster perturbative convergence. Numerical results explicitly illustrate that the axial-vector current contribution is suppressed near the threshold but enhanced at high energies compared to the vector current contribution. Our analytical results are encoded in a Mathematica file that can be conveniently used for precise evaluation of the top quark pair production cross section.

Acknowledgements

We would like to thank Long Chen, Xiang Chen, Xin Guan and Hai Tao Li for helpful discussions. This work was supported in part by the National Science Foundation of China (grant Nos. 12005117, 12175048, 12321005, 12375076) and the Taishan Scholar Foundation of Shandong province (tsqn201909011). The topology diagrams in this paper were drawn using the TikZ-Feynman package [67].

A Topologies of the master integrals

The topology diagrams of the master integrals in the P2 and P3 are displayed below.

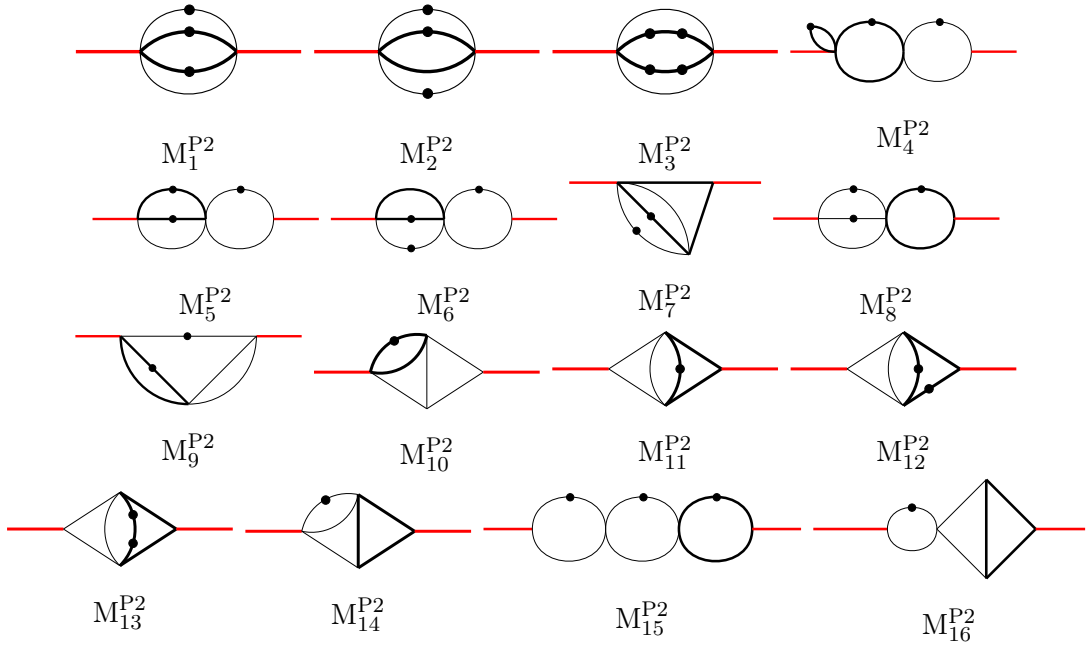


Figure 7: Master integrals in the P2 topology. The thick black and red lines stand for the massive top quark and the vector boson, respectively. One black dot indicates one additional power of the corresponding propagator.

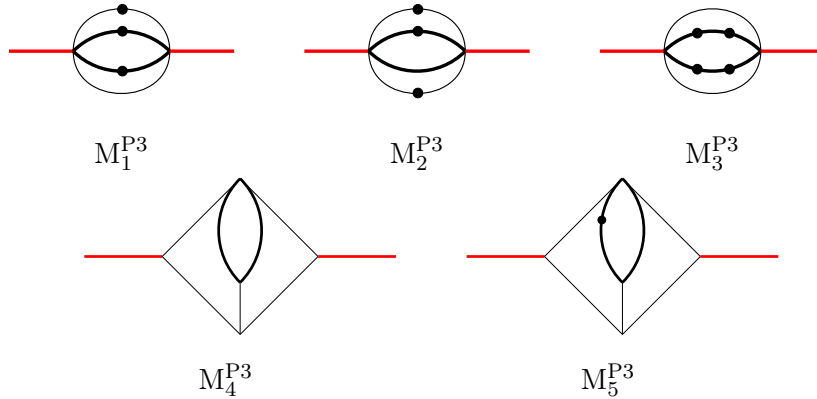


Figure 8: Master integrals in the P3 topology. The thick black and red lines stand for the massive top quark and the vector boson, respectively. One black dot indicates one additional power of the corresponding propagator.

References

- [1] PARTICLE DATA GROUP collaboration, R. L. Workman et al., *Review of Particle Physics*, [*PTEP* **2022** \(2022\) 083C01](#).
- [2] CDF collaboration, F. Abe et al., *Observation of top quark production in $\bar{p}p$ collisions*, [*Phys. Rev. Lett.* **74** \(1995\) 2626–2631, \[\[hep-ex/9503002\]\(#\)\]](#).

- [3] D0 collaboration, S. Abachi et al., *Observation of the top quark*, *Phys. Rev. Lett.* **74** (1995) 2632–2637, [[hep-ex/9503003](#)].
- [4] ATLAS collaboration, *Combination of measurements of the top quark mass from data collected by the ATLAS and CMS experiments at $\sqrt{s}=7$ and 8 TeV*, tech. rep., CERN, Geneva, 2023.
- [5] J. A. Aguilar-Saavedra, *A Minimal set of top anomalous couplings*, *Nucl. Phys. B* **812** (2009) 181–204, [[0811.3842](#)].
- [6] K. Seidel, F. Simon, M. Tesar and S. Poss, *Top quark mass measurements at and above threshold at CLIC*, *Eur. Phys. J. C* **73** (2013) 2530, [[1303.3758](#)].
- [7] T. Horiguchi, A. Ishikawa, T. Suehara, K. Fujii, Y. Sumino, Y. Kiyo et al., *Study of top quark pair production near threshold at the ILC*, [1310.0563](#).
- [8] P. Janot, *Top-quark electroweak couplings at the FCC-ee*, *JHEP* **04** (2015) 182, [[1503.01325](#)].
- [9] M. S. Amjad et al., *A precise characterisation of the top quark electro-weak vertices at the ILC*, *Eur. Phys. J. C* **75** (2015) 512, [[1505.06020](#)].
- [10] A. Czarnecki and K. Melnikov, *Two loop QCD corrections to the heavy quark pair production cross-section in e^+e^- annihilation near the threshold*, *Phys. Rev. Lett.* **80** (1998) 2531–2534, [[hep-ph/9712222](#)].
- [11] M. Beneke, A. Signer and V. A. Smirnov, *Two loop correction to the leptonic decay of quarkonium*, *Phys. Rev. Lett.* **80** (1998) 2535–2538, [[hep-ph/9712302](#)].
- [12] A. H. Hoang and T. Teubner, *Top quark pair production at threshold: Complete next-to-next-to-leading order relativistic corrections*, *Phys. Rev. D* **58** (1998) 114023, [[hep-ph/9801397](#)].
- [13] M. Beneke, A. Signer and V. A. Smirnov, *Top quark production near threshold and the top quark mass*, *Phys. Lett. B* **454** (1999) 137–146, [[hep-ph/9903260](#)].
- [14] M. Beneke, Y. Kiyo, P. Marquard, A. Penin, J. Piclum and M. Steinhauser, *Next-to-Next-to-Next-to-Leading Order QCD Prediction for the Top Antitop S-Wave Pair Production Cross Section Near Threshold in e^+e^- Annihilation*, *Phys. Rev. Lett.* **115** (2015) 192001, [[1506.06864](#)].
- [15] J. Jersak, E. Laermann and P. M. Zerwas, *Electroweak Production of Heavy Quarks in e^+e^- Annihilation*, *Phys. Rev. D* **25** (1982) 1218.
- [16] B. Chokouf e Nejad, W. Kilian, J. M. Lindert, S. Pozzorini, J. Reuter and C. Weiss, *NLO QCD predictions for off-shell $t\bar{t}$ and $t\bar{t}H$ production and decay at a linear collider*, *JHEP* **12** (2016) 075, [[1609.03390](#)].
- [17] W. Beenakker, S. C. van der Marck and W. Hollik, *e^+e^- annihilation into heavy fermion pairs at high-energy colliders*, *Nucl. Phys. B* **365** (1991) 24–78.
- [18] J. Fleischer, A. Leike, T. Riemann and A. Werthenbach, *Electroweak one loop corrections for e^+e^- annihilation into t anti-top including hard bremsstrahlung*, *Eur. Phys. J. C* **31** (2003) 37–56, [[hep-ph/0302259](#)].
- [19] K. G. Chetyrkin, J. H. Kuhn and M. Steinhauser, *Three loop polarization function and $O(\alpha_s^{**2})$ corrections to the production of heavy quarks*, *Nucl. Phys. B* **482** (1996) 213–240, [[hep-ph/9606230](#)].

- [20] K. G. Chetyrkin, R. Harlander, J. H. Kuhn and M. Steinhauser, *Mass corrections to the vector current correlator*, *Nucl. Phys. B* **503** (1997) 339–353, [[hep-ph/9704222](#)].
- [21] R. Harlander and M. Steinhauser, *$O(\alpha_s^{**2})$ corrections to top quark production at e^+e^- colliders*, *Eur. Phys. J. C* **2** (1998) 151–158, [[hep-ph/9710413](#)].
- [22] J. Gao and H. X. Zhu, *Electroweak production of top-quark pairs in e^+e^- annihilation at NNLO in QCD: the vector contributions*, *Phys. Rev. D* **90** (2014) 114022, [[1408.5150](#)].
- [23] J. Gao and H. X. Zhu, *Top Quark Forward-Backward Asymmetry in e^+e^- Annihilation at Next-to-Next-to-Leading Order in QCD*, *Phys. Rev. Lett.* **113** (2014) 262001, [[1410.3165](#)].
- [24] L. Chen, O. Dekkers, D. Heisler, W. Bernreuther and Z.-G. Si, *Top-quark pair production at next-to-next-to-leading order QCD in electron positron collisions*, *JHEP* **12** (2016) 098, [[1610.07897](#)].
- [25] W. Bernreuther, L. Chen, P.-C. Lu and Z.-G. Si, *Top and bottom quark forward-backward asymmetries at next-to-next-to-leading order QCD in (un)polarized electron positron collisions*, *JHEP* **05** (2023) 094, [[2301.12632](#)].
- [26] A. H. Hoang, V. Mateu and S. Mohammad Zebarjad, *Heavy Quark Vacuum Polarization Function at $O(\alpha_s^{**2}(s))$ $O(\alpha_s^{**3}(s))$* , *Nucl. Phys. B* **813** (2009) 349–369, [[0807.4173](#)].
- [27] Y. Kiyo, A. Maier, P. Maierhofer and P. Marquard, *Reconstruction of heavy quark current correlators at $O(\alpha_s^{**3})$* , *Nucl. Phys. B* **823** (2009) 269–287, [[0907.2120](#)].
- [28] X. Chen, X. Guan, C.-Q. He, X. Liu and Y.-Q. Ma, *Heavy-Quark Pair Production at Lepton Colliders at NNNLO in QCD*, *Phys. Rev. Lett.* **132** (2024) 101901, [[2209.14259](#)].
- [29] J. Ma, S.-Q. Wang, T. Sun, J.-M. Shen and X.-G. Wu, *Revisiting the top-quark pair production at future e^+e^- colliders*, *Chin. Phys. C* **48** (2024) 043105, [[2402.02363](#)].
- [30] J. M. Henn, *Multiloop integrals in dimensional regularization made simple*, *Phys. Rev. Lett.* **110** (2013) 251601, [[1304.1806](#)].
- [31] A. B. Goncharov, *Multiple polylogarithms, cyclotomy and modular complexes*, *Math. Res. Lett.* **5** (1998) 497–516, [[1105.2076](#)].
- [32] T. Hahn, *Generating Feynman diagrams and amplitudes with FeynArts 3*, *Comput. Phys. Commun.* **140** (2001) 418–431, [[hep-ph/0012260](#)].
- [33] V. Shtabovenko, R. Mertig and F. Orellana, *FeynCalc 9.3: New features and improvements*, *Comput. Phys. Commun.* **256** (2020) 107478, [[2001.04407](#)].
- [34] V. Shtabovenko, R. Mertig and F. Orellana, *FeynCalc 10: Do multiloop integrals dream of computer codes?*, [[2312.14089](#)].
- [35] S. A. Larin and J. A. M. Vermaseren, *The α_s^3 corrections to the Bjorken sum rule for polarized electroproduction and to the Gross-Llewellyn Smith sum rule*, *Phys. Lett. B* **259** (1991) 345–352.
- [36] S. A. Larin, *The Renormalization of the axial anomaly in dimensional regularization*, *Phys. Lett. B* **303** (1993) 113–118, [[hep-ph/9302240](#)].
- [37] A. V. Smirnov and F. S. Chuharev, *FIRE6: Feynman Integral REduction with Modular Arithmetic*, *Comput. Phys. Commun.* **247** (2020) 106877, [[1901.07808](#)].
- [38] J. Klappert, F. Lange, P. Maierhöfer and J. Usovitsch, *Integral reduction with Kira 2.0 and finite field methods*, *Comput. Phys. Commun.* **266** (2021) 108024, [[2008.06494](#)].

- [39] J. Wang, Y. Wang and D.-J. Zhang, *Analytic decay width of the Higgs boson to massive bottom quarks at next-to-next-to-leading order in QCD*, *JHEP* **03** (2024) 068, [[2310.20514](#)].
- [40] A. V. Kotikov, *Differential equations method: New technique for massive Feynman diagrams calculation*, *Phys. Lett. B* **254** (1991) 158–164.
- [41] A. V. Kotikov, *Differential equation method: The Calculation of N point Feynman diagrams*, *Phys. Lett. B* **267** (1991) 123–127.
- [42] M. Argeri, S. Di Vita, P. Mastrolia, E. Mirabella, J. Schlenk, U. Schubert et al., *Magnus and Dyson Series for Master Integrals*, *JHEP* **03** (2014) 082, [[1401.2979](#)].
- [43] L.-B. Chen and J. Wang, *Analytic two-loop master integrals for tW production at hadron colliders: I **, *Chin. Phys. C* **45** (2021) 123106, [[2106.12093](#)].
- [44] R. N. Lee, *Libra: A package for transformation of differential systems for multiloop integrals*, *Comput. Phys. Commun.* **267** (2021) 108058, [[2012.00279](#)].
- [45] M. Besier, P. Wasser and S. Weinzierl, *RationalizeRoots: Software Package for the Rationalization of Square Roots*, *Comput. Phys. Commun.* **253** (2020) 107197, [[1910.13251](#)].
- [46] X. Liu, Y.-Q. Ma and C.-Y. Wang, *A Systematic and Efficient Method to Compute Multi-loop Master Integrals*, *Phys. Lett. B* **779** (2018) 353–357, [[1711.09572](#)].
- [47] X. Liu, Y.-Q. Ma, W. Tao and P. Zhang, *Calculation of Feynman loop integration and phase-space integration via auxiliary mass flow*, *Chin. Phys. C* **45** (2021) 013115, [[2009.07987](#)].
- [48] X. Liu and Y.-Q. Ma, *AMFlow: A Mathematica package for Feynman integrals computation via auxiliary mass flow*, *Comput. Phys. Commun.* **283** (2023) 108565, [[2201.11669](#)].
- [49] Z.-F. Liu and Y.-Q. Ma, *Determining Feynman Integrals with Only Input from Linear Algebra*, *Phys. Rev. Lett.* **129** (2022) 222001, [[2201.11637](#)].
- [50] H. Ferguson, D. Beiley and S. Arno, *Analysis of PSLQ, an integer relation finding algorithm*, *Math. Comp.* **68** (1999) 351.
- [51] R. N. Lee and A. I. Onishchenko, *ϵ -regular basis for non-polylogarithmic multiloop integrals and total cross section of the process $e^+e^- \rightarrow 2(Q\bar{Q})$* , *JHEP* **12** (2019) 084, [[1909.07710](#)].
- [52] C. Duhr and F. Dulat, *PolyLogTools — polylogs for the masses*, *JHEP* **08** (2019) 135, [[1904.07279](#)].
- [53] J. M. Henn, A. V. Smirnov and V. A. Smirnov, *Evaluating Multiple Polylogarithm Values at Sixth Roots of Unity up to Weight Six*, *Nucl. Phys. B* **919** (2017) 315–324, [[1512.08389](#)].
- [54] H. Frellesvig, D. Tommasini and C. Wever, *On the reduction of generalized polylogarithms to Li_n and $Li_{2,2}$ and on the evaluation thereof*, *JHEP* **03** (2016) 189, [[1601.02649](#)].
- [55] W. Bernreuther, R. Bonciani, T. Gehrmann, R. Heinesch, T. Leineweber, P. Mastrolia et al., *Two-loop QCD corrections to the heavy quark form-factors: Axial vector contributions*, *Nucl. Phys. B* **712** (2005) 229–286, [[hep-ph/0412259](#)].
- [56] W. Bernreuther, R. Bonciani, T. Gehrmann, R. Heinesch, T. Leineweber and E. Remiddi, *Two-loop QCD corrections to the heavy quark form-factors: Anomaly contributions*, *Nucl. Phys. B* **723** (2005) 91–116, [[hep-ph/0504190](#)].
- [57] J. Ablinger, A. Behring, J. Blümlein, G. Falcioni, A. De Freitas, P. Marquard et al., *Heavy quark form factors at two loops*, *Phys. Rev. D* **97** (2018) 094022, [[1712.09889](#)].

- [58] M. Beneke, J. Piclum and T. Rauh, *P-wave contribution to third-order top-quark pair production near threshold*, *Nucl. Phys. B* **880** (2014) 414–434, [[1312.4792](#)].
- [59] K. G. Chetyrkin, J. H. Kuhn and M. Steinhauser, *RunDec: A Mathematica package for running and decoupling of the strong coupling and quark masses*, *Comput. Phys. Commun.* **133** (2000) 43–65, [[hep-ph/0004189](#)].
- [60] F. Herren and M. Steinhauser, *Version 3 of RunDec and CRunDec*, *Comput. Phys. Commun.* **224** (2018) 333–345, [[1703.03751](#)].
- [61] M. Beneke, Y. Kiyo, A. Maier and J. Piclum, *Near-threshold production of heavy quarks with QQbar_threshold*, *Comput. Phys. Commun.* **209** (2016) 96–115, [[1605.03010](#)].
- [62] D. J. Broadhurst, N. Gray and K. Schilcher, *Gauge invariant on-shell Z(2) in QED, QCD and the effective field theory of a static quark*, *Z. Phys. C* **52** (1991) 111–122.
- [63] N. Gray, D. J. Broadhurst, W. Grafe and K. Schilcher, *Three Loop Relation of Quark (Modified) Ms and Pole Masses*, *Z. Phys. C* **48** (1990) 673–680.
- [64] P. Marquard, A. V. Smirnov, V. A. Smirnov and M. Steinhauser, *Quark Mass Relations to Four-Loop Order in Perturbative QCD*, *Phys. Rev. Lett.* **114** (2015) 142002, [[1502.01030](#)].
- [65] P. Marquard, A. V. Smirnov, V. A. Smirnov, M. Steinhauser and D. Wellmann, *$\overline{\text{MS}}$ -on-shell quark mass relation up to four loops in QCD and a general $SU(N)$ gauge group*, *Phys. Rev. D* **94** (2016) 074025, [[1606.06754](#)].
- [66] M. Beneke, *Renormalons*, *Phys. Rept.* **317** (1999) 1–142, [[hep-ph/9807443](#)].
- [67] J. Ellis, *TikZ-Feynman: Feynman diagrams with TikZ*, *Comput. Phys. Commun.* **210** (2017) 103–123, [[1601.05437](#)].